Mine Water and the Environment
https://doi.org/10.1007/s10230-024-01020-1

TECHNICAL ARTICLE

Combining UAS-TIR and GEM-2 Techniques for Focused Water Sampling and Isotope Geochemical Analysis at Two Mine Sites in Northern Finland

Juuso Ikonen[1] · Anssi Rauhala[2] · Anne Tuomela[2] · Heini Postila[3] · Timo Kumpula[4] · Pasi Korpelainen[4] · Raija Pietilä[1] · Riku-Olli Valta[5] · Jouni Lerssi[6] · Hannu Panttila[1] · Kirsti Korkka-Niemi[1]

Received: 23 April 2024 / Accepted: 26 December 2024

Abstract

A combination of thermal infrared (TIR) images captured by uncrewed aircraft systems (UASs) and manual geophysical measurements with a GEM-2 device were used to better plan a water sampling campaign at an abandoned Au-Cu mine and an active Ni-Cu-PGE mine in the sub-arctic boreal zone in northern Finland. Anomalies from the TIR images and GEM-2 conductivity values were used to focus the water sampling. The hydrogeochemistry and isotopic compositions of oxygen ($\delta^{18}O$), hydrogen ($\delta^{2}H$), strontium ($^{87}Sr/^{86}Sr$), and sulfur ($\delta^{34}S$) were analyzed to better understand the flow regime of possible effluent waters at these mine sites. The TIR images were useful in pinpointing sites where groundwater and surface water were potentially interacting. This was confirmed with the oxygen and hydrogen isotopic data. Isotopic values for the two groundwater solutes used here (Sr and S), reflected the local geology and the biogeochemical environment at the mine sites. The electrical conductivity values obtained from the GEM-2 measurements were influenced by the local geochemistry, particularly the presence of conductive sulfide-bearing paraschist rock. The anomalies from the UAS-TIR and GEM-2 data revealed sampling sites well suited for tracking potential effluent waters at the two mine sites.

Keywords Geophysics · Hydrogeology · Boreal · Stable Isotopes · Strontium · Sulfur · Hydrogeochemistry

Introduction

Sustainable mining focuses on avoiding harmful effects on the environment in each step of the mine life cycle from prospecting to mine closure and long-term rehabilitation and monitoring. Therefore, widespread monitoring and multiple techniques are used to monitor the effluent flow paths (Banerjee et al. 2015; Larkins et al. 2018; Turunen et al. 2020). Traditionally this is done by water sampling in situ, but because the mine sites typically cover vast areas, the development of remote sensing methods and sensor-based online monitoring offers novel prospects to mine monitoring (Almeida et al. 2022; Choe et al. 2008; Isokangas et al. 2019; Karan et al. 2016; McKenna et al. 2020; Minh and Dung 2023; Rauhala et al. 2017; Sares et al. 2004; Swayze et al. 2000; Winkelmann et al. 2001).

When the aim is to understand the impact of mining waters to a watershed, one important factor is the water flow paths in the mining area. Information about hydrological processes and groundwater surface water interaction can be explored with temperature anomalies (Andersson

✉ Juuso Ikonen
juuso.ikonen@gtk.fi

1 Geological Survey of Finland, Water and Mining Environment Solutions, Vuorimiehentie 5, 02150 Espoo, Finland

2 Civil Engineering, University of Oulu, P.O. Box 4200, 90014 Oulu, Finland

3 Water, Energy and Environmental Engineering, University of Oulu, P.O. Box 4300, 90014 Oulu, Finland

4 Department of Geographical and Historical Studies, University of Eastern Finland, 80101 Joensuu, Finland

5 Geological Survey of Finland, Environmental Solutions, Lähteentie 2, 96100 Rovaniemi, Finland

6 Geological Survey of Finland, Geophysical Solutions, Viestikatu 7 A, PL 1237, 70211 Kuopio, Finland

Published online: 10 January 2025

2005; Isokangas et al. 2019; Rautio et al. 2018), especially in the late summer when surface water temperatures differ the most with groundwater temperatures in boreal environments (Anderson 2005). In a large mine area, manual temperature measurements are laborious, time-consuming, and sometimes difficult. However, by utilizing an uncrewed aircraft system (UAS) for thermal infrared (TIR) imaging, the process becomes feasible and easier to manage, as well as minimizing risks to personnel and ensuring secure data collection. Thus, interpreting TIR images is a cost-effective way to produce information on a large scale (Rautio et al. 2018).

Combining geophysical survey techniques with the TIR data enables further extraction of useful information. Soil electrical conductivity (EC) is known to correlate with many soil properties (Grisso et al. 2009; Huang et al. 2003; McNeill 1980; Witten et al. 1997). GEM-2 is a broadband electromagnetic (EM) sensor that is well suited for shallow environmental characterization (Won et al. 1996). GEM-2 measurements have been used in various environmental investigations including underground (UXO)-detection, peat thickness investigations, and tracking seepage water paths in mining environments (Alakangas et al. 2019; Boaga et al. 2020; Lerssi et al. 2016; Valjus et al. 2017). By integrating the TIR orthomosaics with the GEM-2 data and available soil maps, illustrative analysis of the possible contaminated areas can potentially be made. The combination can indicate places where different waters have mixed, which can cause changes in EC values. These types of preliminary studies have not been published from sub-arctic mine sites previously. Overall, studies that integrate remote sensing with geophysical methods are relatively rare.

Further knowledge on the pathways of surface mine waters can be attained by adding the TIR and GEM-2 data to the information from the hydrogeochemical and isotopic analyses of selected elements from the sampled waters in the study area (Isokangas et al 2019; Pellicori et al. 2005). Hydrogeochemical indicators have been used for decades to verify the observed GW – SW connections (Conant 2001; Hayashi and Rosenberry 2002; Hinton et al. 1994; Kendall and Coplen 2001; Kenoyer and Anderson 1989; Korkka-Niemi et al. 2012; Krabbenhoft et al. 1990; Rautio and Korkka-Niemi 2015). The use of stable isotopic compositions of hydrogen and oxygen ($\delta^{18}O$, $\delta^{2}H$) has been demonstrated to be an applicable method in GW – SW interaction studies when there is a sufficient differentiation of end members (Hinton et al. 1994; Krabbenhoft et al. 1990; Rautio and Korkka-Niemi 2015; Rautio et al. 2015).

Environmental isotope compositions from water samples are analyzed to track variations due to fractionation by different biological and geochemical processes, or anthropogenic factors such as mining, or due to locality, e.g. geology. Thus, information on the origin of water, hydrological dynamics, or mixing of different water types can be gained. With the fractionation that occurs during physical processes, the isotopic compositions of hydrogen ($^{2}H/^{1}H$) and oxygen ($^{18}O/^{16}O$) enable differentiation between surface- and groundwaters during the hydrological cycle (Dansgaard 1964; Qu et al. 2023). The isotopic compositions of hydrogen and oxygen in the Finnish groundwaters are that of the mean weighted average composition of the local precipitation (Kortelainen and Karhu 2004). With strontium, the isotopic composition (expressed as $^{87}Sr/^{86}Sr$) reflects the sum of local mineral matter, with negligible fractionation by biological or chemical processes (Shand et al. 2009). Isotopic composition of sulfur, $\delta^{34}S$, is affected by fractionations in mass-dependent chemical and microbial processes, the main process being bacterial sulfate reduction (BSR; Canfield 2001; Faure and Mensing 2005). Unlike strontium, sulfur is a non-conservative isotopic tracer. By combining the different isotopic compositions to a site-specific hydrology, hydrogeochemistry, geochemistry, and geology, it can be possible to formulate a conceptual model of the pathways and mixing of waters in the study area and gain information on the biogeochemical processes along the flow paths. In mining areas, isotopes can be used to better understand the hydrogeochemical conditions and flow paths of local waters (Pellicori et al. 2005; Rautio et al. 2018).

Mining environments require understanding of the geological complexity of the area. Our objective in this study was to improve monitoring of waters in both closed and active mining environments to facilitate focusing and optimizing sampling in vast mining areas. To achieve this, we: 1) assessed combining remote sensing and geophysical measurements (TIR, GEM-2) in order to help design the water quality sampling plan, 2) focused the in-situ sampling on the places identified by the combined analysis of TIR images and GEM-2 data, and 3) tested the plan with the help of hydrogeochemistry and isotopic compositions of H, O, Sr, and S from the sampled waters to look at what useful additional information the use of these isotopes might bring.

Study Sites

The Closed Saattopora Mine

The closed Saattopora mine (67.79° N, 24.41° E) is in the Kittilä municipality in northern Finland (Fig. 1). The mine operated from 1988 to 1995 and produced gold (Au) and copper (Cu). The area is situated in the lowlands of Finnish Lapland's fell region and the Saattopora mine site is ≈ 230 to 260 m above sea level. The study site is in the Finnish sub-arctic and is mostly covered by boreal forest. Based on weather data from 2010–2021, the annual average

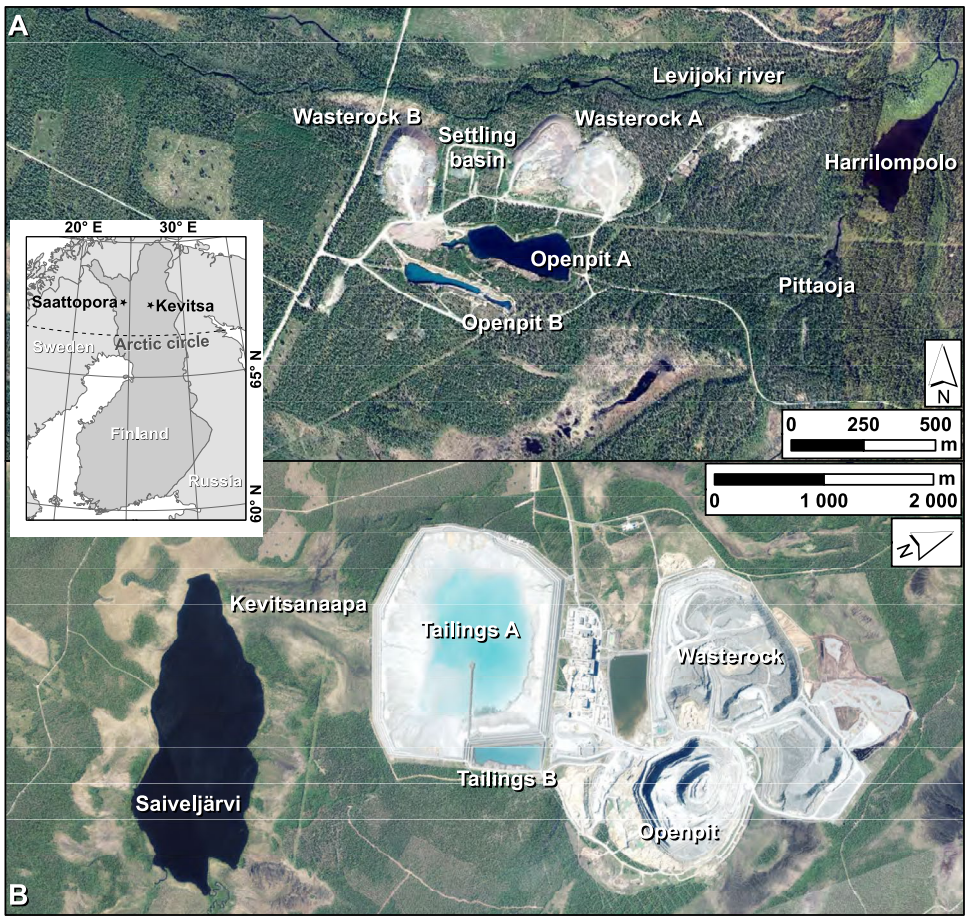

Fig. 1 Overview of the **A** Saattopora and **B** Kevitsa mine sites and their location in Finland in the inset (Aerial images: National Land Survey of Finland 2023)

temperature in Kittilä area (measured at the Kittilä Center) is 0.7 °C, and the average precipitation is 577 mm (Finnish Meteorological Institute (FMI) 2022). The average evapotranspiration was between 200 and 300 mm during the years 1961–1990 (Solantie and Joukola 2001).

The largest river in the study area, just north of the mine area, is the eastward-flowing Levijoki (Fig. 1A), which has a total length of 40.6 km and a total runoff area of 397 km^2. Most of the surface water and groundwater runoff from the mine area ends up in Levijoki. The closest lake is Harrilompolo, located ≈ 750 m east of the eastern waste rock pile. There is also a small brook, Pittaoja, that runs in a north-east direction into the lake Harrilompolo. The soil in the area consists of sandy till, sand and gravel deposits, peat, and bedrock outcrops. The peatlands are mainly *Carex*-containing bogs, which in the area include eutrophic fens to some extent. The thickness of the top peat layer of the till ranges between 0–70 cm in the area between the waste rock pile B and river Levijoki, being thickest near the river, and containing plenty of boulders (Alakangas et al. 2019). The overburden was measured by soil drilling as 8.5 m thick near the western waste rock pile (Alakangas et al. 2019).

The bedrock of the area is defined as belonging to the Savukoski group, which is part of the paleoproterozoic Central Lapland Greenstone Belt (CLGB). The Savukoski group entails fine-grained metasedimentary and pyroclastic rocks, such as graphite-bearing phyllites, black schists, tuffs, and tuffites (Lehtonen et al. 1998; Rastas et al. 2001). Mafic tuffs and lavas are found in the northern, northeastern, and southwestern parts of the mine area, and phyllites and mica schists in the western and southeastern parts. Komatites and some intrusive diabase dykes are also present. The Saattopora ore deposit contained gold along with copper, sulfides (pyrrhotite and pyrite), and U-Th oxides (Alakangas et al. 2019). The bedrock in the area is intersected by a long, nearly east–west trending fault zone; the weathered bedrock above the solid bedrock is less than 1 m thick (Alakangas et al. 2019; Molnar et al. 2019).

A total of 2.12 Mt of Cu-Au ore and 3.7 Mt of waste rock was extracted from Saattopora during 1988–1995 and the ore was transported elsewhere for processing (Korkalo 2006). The ore was mined from two open pits (A and B) until 1992, after which mining continued underground in open pit B (Korvuo 1997). The waste rock was stacked into two piles located north of the open pits (Fig. 1A). The two piles lay on top of till apart from the northern

parts of pile B that are partly on top of peat-covered till. A settling basin located between the waste rock piles was used for dewatering of the open pits. A ditch that was excavated to collect seepage waters from waste rock pile B is located between the settling basin and the western pile (Fig. 1A). The ditch extends from the waste rock area to the river Levijoki. According to the mineralogical results, the Saattopora waste rock samples are mainly silicate minerals, together with carbonates, some oxides, and sulfides (Alakangas et al 2019).

The Active Kevitsa Mine

The Kevitsa Ni-Cu-PGE mine (67.69° N, 26.96° E) is in central Lapland in the municipality of Sodankylä, ≈ 35 km north of the Sodankylä village (Fig. 1). Open pit mining started in June 2012 and is expected to continue until 2034 (Boliden 2022). Based on weather data from 2010–2021, the annual average temperature in Sodankylä area (measurement point in Sodankylä, Tähtelä) is 0.8 °C and the average precipitation is 555 mm (FMI 2022). The average evapotranspiration was between 200 and 300 mm in the years 1961–1990 (Solantie and Joukola 2001).

South of the mine area lies a peatland, Kevitsanaapa, which is a partly treeless wet mire with several springs. There is a small brook from the tailings pond towards the lake Saiveljärvi to the south. The mine area lays mainly on top of one watershed with the runoff flowing west towards the river Kitinen. The most southern and southeastern parts of the mine area belong to a watershed where runoff flows towards the east and south (Pöyry 2011).

The mine is situated in the central Lapland ice divide zone and the area is defined by vast bog areas alongside some separate fells. Glacial erosion in the area has been relatively minor, which has resulted in only a few bedrock outcrops and noticeable soil thickness (20–30 m) (Manninen et al. 1996). Due to the location, elevation differences are also relatively small, ranging between 220–310 m above sea level in the area (Pietilä et al. 2014). The average soil thickness is 5 m, and it is mainly till (Pöyry 2011). In low-lying areas, like Kevitsanaapa, the topmost soil layer is usually *Carex* peat, between 0.2 and 3.4 m thick (Pöyry 2011).

The Kevitsa Ni-Cu-PGE sulfide ore is part of the Kevitsa magmatic and mafic–ultramafic intrusion deposit. The intrusion consists of a northern ultramafic part and southern gabbrophyre and gabbro parts (Santaguida et al. 2015). The ore is hosted within the ultramafic part and is disseminated in sulfide minerals, mainly in olivine-pyroxenite rocks (Santaguida et al. 2015). The waste rock consists of olivine-pyroxenites, olivine-websterites, gabbros, and dunites. The bedrock further from the deposit contains graphite schists in the southern parts of the tailings pond region and the Kevitsanaapa area (Santaguida et al. 2015). In places, the surface bedrock in the area is fractured and the rock types around the intrusion, such as shales and quartzites, are often very fractured (Pöyry 2011). The area is dominated by a northeastern compression, which means that the north-east trending fractures may be open and act as water flow paths (Pöyry 2011).

The mine structures include an open pit, waste rock area, processing facilities, and a TSF consisting of two separate ponds and water-processing systems, including a run-off field, settling basin, and water reservoirs (Fig. 1B). Low-sulfide waste material is stored in the main tailings pond A located south of the mine. The sulfide-rich tailings is stored separately in pond B, which is located N-E and next to the main tailings pond. The study site is in the Kevitsanaapa peatland, which is between the TSF and the lake Saiveljärvi, south of the mine.

Materials and Methods

UAS Surveys

UAS data was collected at the Saattopora site in the afternoon of August 26, 2020, in cloudy to overcast conditions. The available 10 min weather station data from the Kittilä Airport, some 22 km southeast of the Saattopora mine, reported air temperatures of 12.0–13.4 °C (mean 12.7 °C). The TIR data was captured utilizing a DJI Matrice 210 UAS and a DJI Zenmuse XT thermal camera with a 640 × 512 sensor resolution and a 13 mm lens. A total of 2453 TIR-images were collected from a flight height of ≈ 1–50 m, covering an area of ≈ 1.8 km^2 (Fig. 2A). RGB imagery was collected utilizing a DJI Phantom 4 RTK UAS equipped with a 1 inch 20 Mpix sensor and 24 mm (35 mm equivalent) lens. The DJI Phantom 4 RTK utilizes two GNSS (global navigation satellite system) receivers and a real-time kinematic (RTK) solution to improve the GNSS positioning accuracy of the UAS down to a level of few centimeters, compared to an accuracy of a few meters obtained with an autonomously operating single-frequency GNSS receiver (Tomaštík et al. 2019). A total of 1550 RGB-images were collected from a flight height of ≈ 145 m, covering an area of ≈ 2.4 km^2.

At the Kevitsa site, UAS data was collected in the afternoon of August 17, 2021, in mostly cloudy or overcast conditions. Reported air temperatures at the Sodankylä weather station, some 35 km north-northwest from the site, were 12.3–14.0 °C (mean 13.2 °C) during the flights. The data was collected utilizing a DJI Matrice 300 RTK multicopter and DJI Zenmuse H20T multisensor payload that includes a 640 × 512 pixel thermal camera with a 13.5 mm focal length and an 1/2.3 inch 12 Mpix wide angle RGB camera with a 24 mm focal length (35 mm equivalent). A total of 3287 TIR images and 3287 RGB images were collected from a flight

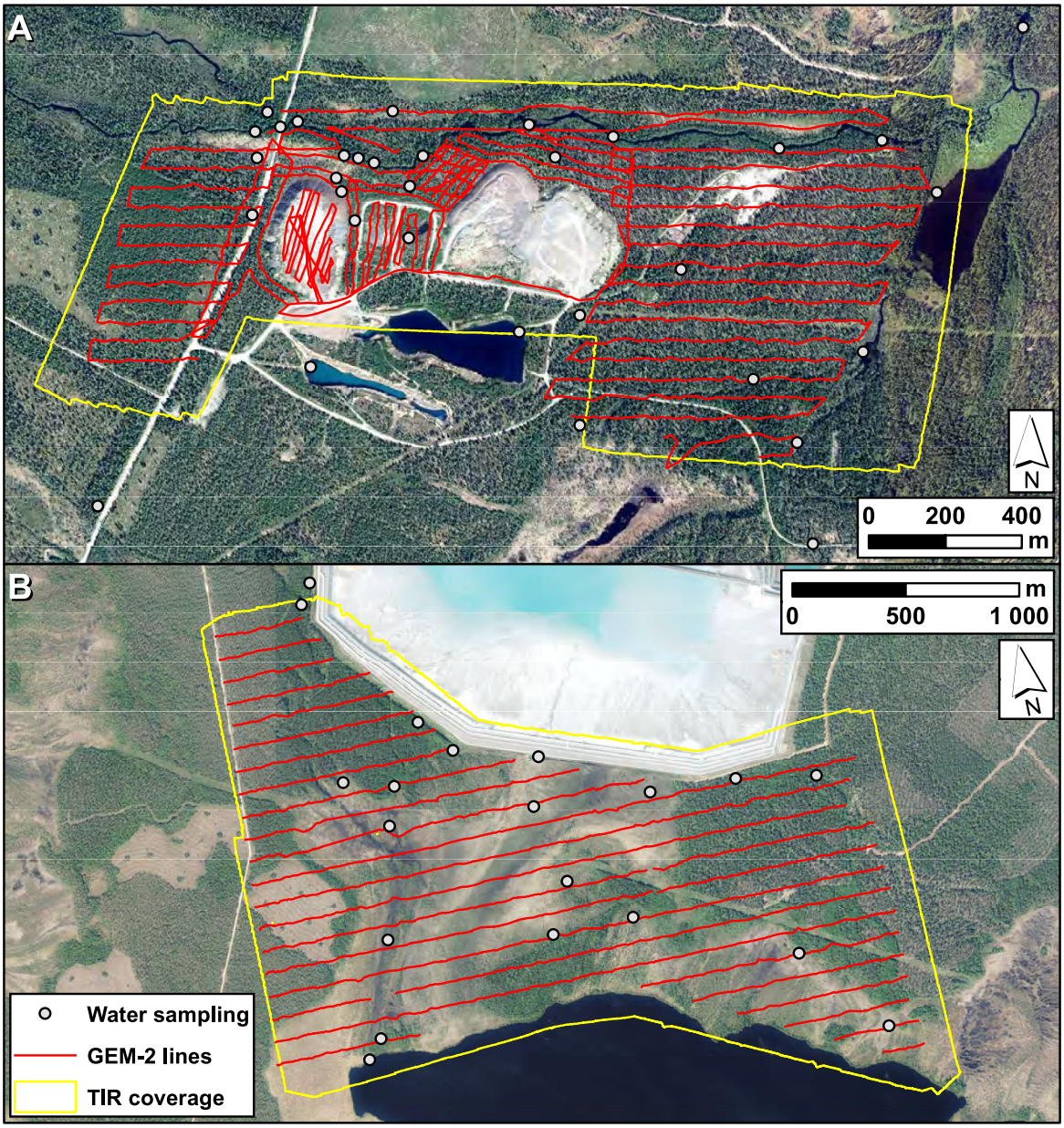

Fig. 2 Thermal infrared (TIR) coverage, GEM-2 survey lines, and water sampling locations at the **A** Saattopora and **B** Kevitsa sites

height of ≈ 240 m, covering areas of ≈ 4.7 km^2 (Fig. 2B) and ≈ 5.5 km^2, respectively.

Both TIR and RGB imagery were processed utilizing Agisoft Metashape Professional. The ground sampling distances (GSD) for the resulting TIR and RGB orthomosaics for the Saattopora site were ≈ 18.7 cm and ≈ 3.7 cm, respectively. Corresponding GSDs for the Kevitsa site were ≈ 20.6 cm and ≈ 7.8 cm. The georeferencing of the TIR orthomosaics were improved manually in ESRI ArcGIS 10.7 with the help of the more accurate RGB orthomosaics.

The TIR data was processed as a grayscale mosaic having brightness values (BV) of 0–255. The use of such relative temperature rather than specific (absolute) temperature allows mapping potential temperature anomalies but does not require sensor calibration and correction of local air temperature, relative humidity, reflective temperature, etc. A similar method has been utilized by multiple hydrological studies (Autio et al. 2023; Dugdale et al. 2019; Glaser et al. 2018; Isokangas et al. 2019). The dataset was then analyzed by visual inspection to locate cold spots indicating potential locations of groundwater seepage. This information was further studied along with the GEM-2 results and a preliminary sampling plan was created. In this preliminary analysis combining the TIR imagery and GEM-2 data, the anomalies

were classified as having only a temperature anomaly, or as having a temperature anomaly and an electro-magnetic anomaly (EC anomaly) due to mineralization, or possible locations of contaminated seepage waters.

GEM-2 Surveys

The GEM-2 is a hand-held, digital, multi-frequency electromagnetic sensor. The current iteration of the sensor operates over a frequency range of ≈ 300 Hz to 93,000 Hz and can transmit an arbitrary waveform containing multiple frequencies. Three to five simultaneous measuring frequencies are recommended, enough to get the necessary information from different depths corresponding to those frequencies (Yaccup and Brabham 2012). The unit uses the pulse-width modulation technique to transmit and receive any digitally synthesized waveform (Huang et al. 2003; Witten et al. 1997; Won et al. 1996). GEM-2 has a separation of 1.66 m between the transmitter and receiver. Maximum depth of exploration is ≈ 10 m depending on ground conductivity, target volume, and ambient electromagnetic noise. At normal walking speed, station spacing along the line is ≈ 10 cm. The location was recorded via a GNSS receiver.

The GEM-2 measurements at the Saattopora study site were conducted during a previous project in August 2017 and 2018 (Alakangas et al. 2019) and expanded and completed for this study in August of 2020 (Fig. 2A). The measurements at the Kevitsa study site were conducted in August of 2020 (Fig. 2B). The GEM-2 results were processed, combined, and interpolated using the Oasis Montaj software. The GEM-2 EC is referred to as the apparent conductivity and was computed from the responses of four different measurement frequencies: 1475, 5825, 22,225, and 75,525 Hz, to get an average apparent conductivity from the depths corresponding to the frequencies used. This was done using the EMInventor software provided by Geophex Ltd. The final maps were made using ArcGIS 10.7.

The high frequency (75,525 Hz) results are shown and discussed separately. This high frequency quadrature component is most sensitive to topsoil conductivity changes while the lower frequencies travel deeper into the soil structures. At high frequencies, especially the quadrature component, is better able to obtain the elevated values caused by slightly increased topsoil conductivity (Won et al. 1996).

Hydrogeochemistry

Water sampling in Saattopora

Water samples were collected from the Saattopora study area as part of a previous project between the years 2016–2018, described in depth in Alakangas et al. (2019), and expanded in this study during the 8th and 9th of September 2020. At the Saattopora site, there are four groundwater observation wells (GW1–GW4). A fifth observation well (GW5), located 0.5 km southwest of the mine site, provides a groundwater reference sample. In addition to groundwater samples, surface water sampling sites in 2016–2018 were selected to detect potential impacts of the mine as well as to provide knowledge on the geochemical state of the nearby water bodies. The sampling in 2016 was done in August and September, and in 2017 in September (Fig. 3.). The 2018 sampling was conducted in June. During these field visits, temperature (T), dissolved oxygen (DO), pH, EC, and oxygen reduction potential (ORP) were determined using a portable multi-parameter YSI Professional Plus sonde (supplemental Table S-1).

The water sampling points in September 2020 at the Saattopora site were selected based on the results of GEM-2 electromagnetic measurements, visually detected cold spots from TIR-images, along with geological knowledge of the area. A total of 19 water samples were collected. The field parameters in 2020 were measured with WTW Multi 350i (Table S-1).

Sampling site locations categorized by year are shown in Fig. 3. Appropriate sample pretreatment, filtering, and acidification were done in the field after sampling. Treated samples were stored in a cold container during field work and transportation to the laboratory. In summary, a total of 45 samples were collected from 34 different locations in the study area between the years 2016 and 2020.

Water sampling in Kevitsa

The sampling campaign at Kevitsa was on the 31st of August and the 1st of September in 2021. The 20 samples were collected after studying the anomalies from the TIR-images and the GEM-2 measurements as with the Saattopora site (Fig. 3). The field measurement data can be found in supplemental Table S-2. Four groundwater observation wells (GW1–GW4) were selected for sampling near the tailings storage facility (TSF). These wells were sampled using a bailer. Two additional groundwater samples were collected from springs (GW5, GW6). The water sample MW1 was taken from a small pool near the TSF, which collects waters from the facility. Surface water samples were collected from forested areas (FPW1–FPW5, forest pond water) and from the boggy (for the most part treeless) area at the study site (BPW1–BPW7, bog pond water) as well as from the lake Saiveljärvi (LW1). The natural brook that runs from the mine site towards the lake Saiveljärvi was seen as a prominent sampling area (BPW1, BPW2,

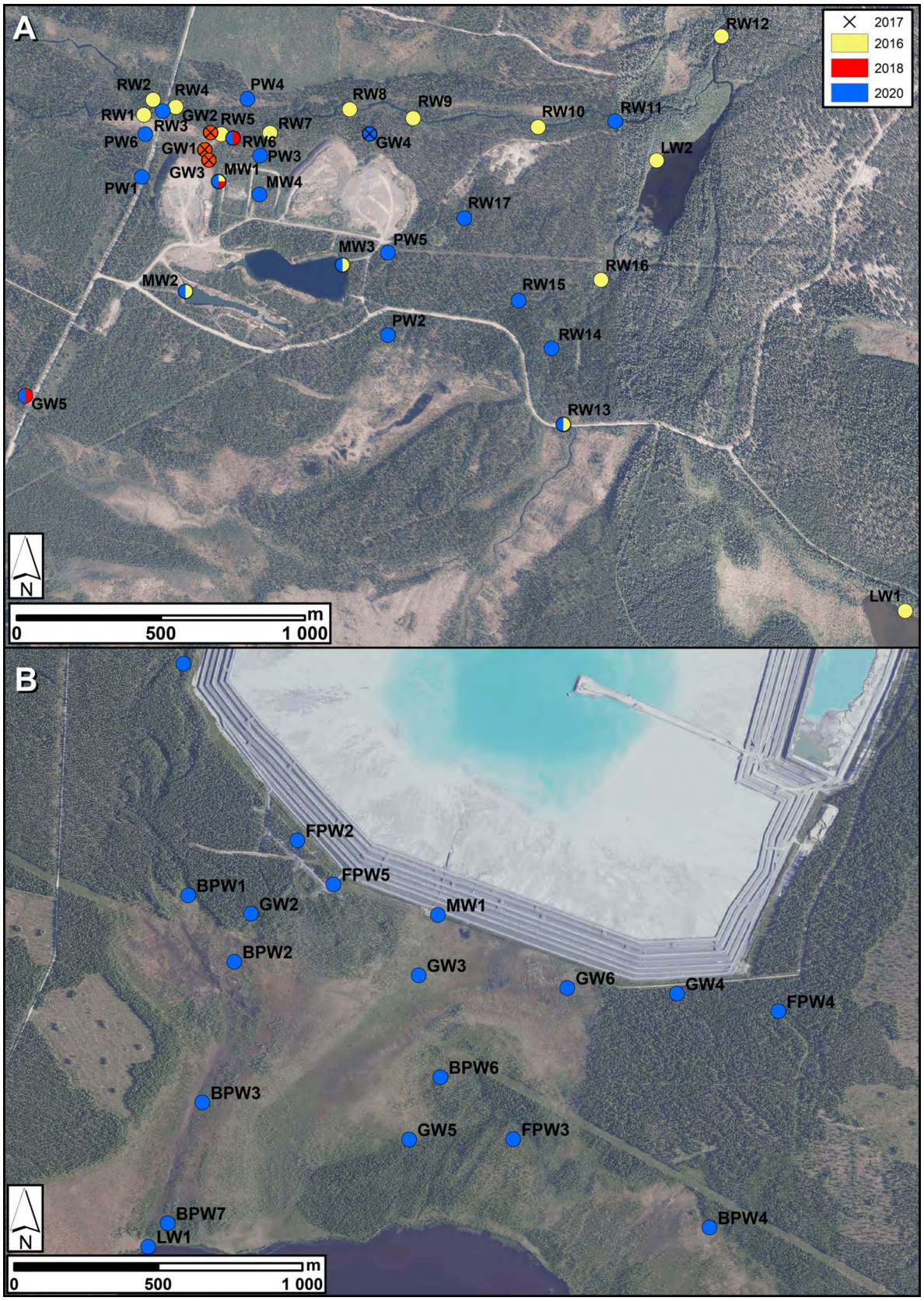

Fig. 3 Water sampling locations in Saattopora **A** and Kevitsa **B**

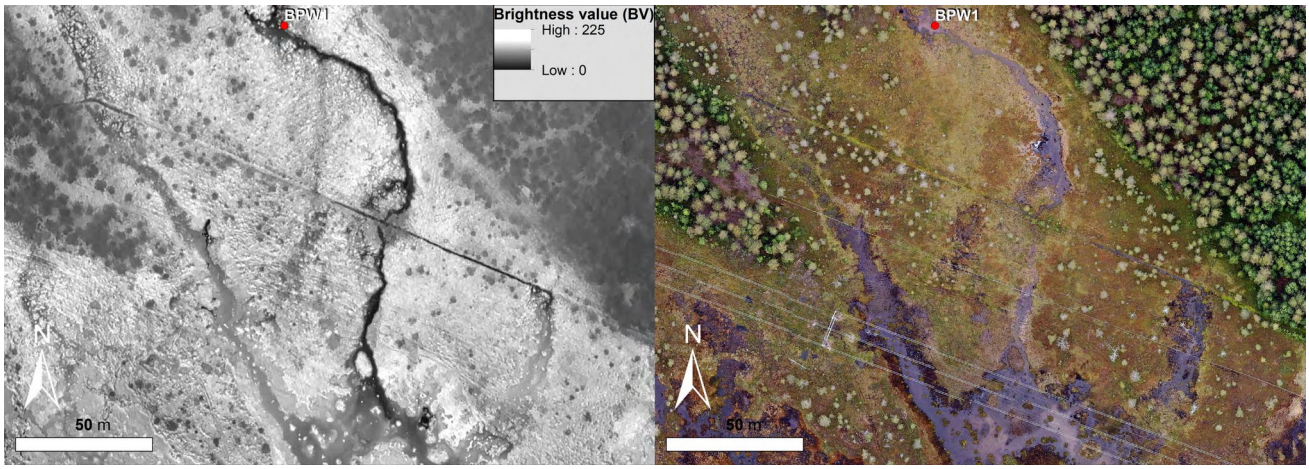

Fig. 4 Discharging groundwater seen in the TIR-image (left) with lower brightness value indicating lower temperatures with darker color

BPW3, BPW7) as it is known to be a channel for surface and discharged groundwater flow due to the local topography. Field parameters were measured with YSI EXO1 multiparameter sonde and sample treatment was carried out as described above for the sampling in Saattopora.

Laboratory analyses and statistical treatment of data

The hydrogeochemical laboratory tests for the water samples from both study sites were done in the accredited laboratory Eurofins Labtium Oy in Espoo. Sampling pretreatment and analysis methods are shown in detail in supplemental Table S-3. The laboratory analysis methods were the same for the water samples collected at the Saattopora study site during 2016–2018 (Alakangas et al. 2019), where water samples were analyzed by Labtium Oy laboratory using ICP-OES and ICP-MS for dissolved elements, ion chromatography following SFS-EN ISO 10304–1 for anions (Br, Cl, F, SO_4, NO_3), and SFS-EN ISO 15681–1 for PO_4. The isotopic analyses for oxygen and hydrogen were performed with a Picarro L2130-i device (Picarro Inc., Santa Clara, CA, USA), and a plasma multi-collector ICP-MS (Nu Instruments, Wrexham, UK) was used for the isotopic analyses of strontium and sulfur. The isotopic analyses methods are described in more detail in the supplemental material.

The laboratory results from the analyses of the water samples were statistically correlated and analyzed with SPSS (IBM SPSS Statistics 2013). The Pearson correlation coefficients were calculated to establish relationships between the EC measured in waters in the field and the EC interpreted from the GEM-2 produced EC data. A hierarchical cluster analysis (HCA) performed with SPSS using Ward's method and squared Euclidean distance included main ions, alkalinity, pH, and EC for Saattopora and for Kevitsa main ions and EC in addition to Ni, Sr, and Co. The data was normalized using Log10-transfomation prior to HCA, excluding pH and alkalinity in the Saattopora data and EC and Cl in the Kevitsa data, which already had statistically symmetrical (normal) distribution. A principal component analysis (PCA) was also conducted for the datasets from both study sites. Data analysis for the isotopic compositions were performed with Microsoft Excel for cross-plots and basic calculation.

Results

Hydrogeochemistry of Sampled Waters

UAS Survey

The mean air temperature during flights was 12.7 °C in Saattopora (data from Kittilä Airport) and 13.2 °C in Kevitsa (data from the Sodankylä weather station). The surface water temperatures were measured on-site a week after TIR data collection and were between 8.9 – 13.1 °C (Levijoki, Pittaoja, and quarry ponds) for the Saattopora site. In Kevitsa, the nearby lake Saiveljärvi was measured at 11.8 °C, similarly a week after the flight.

As actual temperature values were not applicable from the TIR data without e.g. sensor calibration, the relative temperatures that the TIR data presented were given as brightness values (BV 0 –255). Lower BV values (darker in color) represent lower temperatures and vice versa (Fig. 4). The produced TIR orthomosaics are shown in supplemental

Fig. S-1. A clear temperature difference between the local groundwater temperature (3–4 °C, Hietula 2018) and the surface water and air temperatures made it possible to detect cold temperature anomalies caused by e.g. groundwater seepage (Fig. 4). Cold spots can be seen in the TIR-orthomosaic image where groundwater is discharged either in springs or brooks (Figs. 5 & S-1).

Areas where discharging groundwater mixes with surface water can also be distinguished from the TIR data. This kind of mixing is clearly seen in the upstream parts of a brook at the Kevitsa study site that is situated in the bog area (Fig. 4). In this area, discharging groundwater from the BPW1 site merges with surface water downstream at a location where the brook is the widest. Four closeups of temperature anomalies from both study sites are shown in Fig. 5, where the isotopic compositions of hydrogen and oxygen of the sampled waters demonstrated a clear groundwater influence (Fig. S-1, supplemental Table S-4).

GEM-2

Saattopora

GEM-2 EC and the high frequency (75,525 Hz) quadrature component maps are presented in Figs. 6 and 7 with bedrock geology at the Saattopora study site. Figure 6 displays only the areas with noticeable conductivity anomalies. A correlation between the bedrock and GEM-2 anomalies can be observed, e.g. near the RW16 sampling point and west of RW17 (Fig. 6). The sandy formation near the river Levijoki at the northeastern sector of the study area near sampling point RW10 is seen as a homogeneous anomaly where EC values are uniformly lower in the high frequency GEM-2 data (Fig. 7). Slight variations in the conductive values show up at this area (Fig. 6), which could be explained by the elevated conductivity values in the water-saturated soils near the river. The conductivities of the dry and water-saturated geological material are presented in supplemental Table S-5. Both the GEM-2 EC and high frequency maps display a noticeable anomaly between the waste rock piles and the river Levijoki near the sampling points GW2 and RW5 as well as GW4 (Figs. 6 and 7). Similar findings were reported in the previous measurements by Alakangas et al. (2019). The strong anomaly seen in the high frequency map in Fig. 7 near sampling points RW1 and RW2 was caused by the metallic bridge crossing the river at that location.

Kevitsa

GEM-2 EC and the high frequency (75,525 Hz) quadrature component maps are presented in Figs. 8 and 9 with bedrock geology at the Kevitsa study site. As with Saattopora, the bedrock influence on the GEM-2 conductivity values is noticeable. This can be seen for instance in the northwestern part of the study area south of the sampling point FPW1, in the middle of the study area west of GW3 and GW5, and to the east near the sampling points FPW4, BPW4, and BPW5 in Fig. 8, which displays the apparent conductivity values with lower frequencies that travel deeper in the sediment matter, thus reflecting the bedrock influence more. The high frequency quadrature component map in Fig. 9 shows higher values along the ditch running south towards the lake Saiveljärvi (Figs. 3 & S-1), which is also seen in the elevated conductivity values of the sampling points BPW2, BPW3, and BPW 7, as well as some groundwater seepage points, e.g. in the bog area west of the sampling point GW5.

Field measurements

Saattopora Field measurements of pH, EC, ORP, DO, and temperature are shown in Tables S-1 and S-2. In Saattopora, the groundwater samples from the observation wells in the study area (GW1–GW5) show a pH range of 5.7–7.2. The pH values for samples of observation wells GW4 and GW5 were measured in the lab due to problems with the pH sensor in the 2020 sampling. The surface water samples (MW1–MW4, PW1–PW6, RW3–RW17) have a higher pH range, 6.9–8.0.

The EC values varied considerably within cluster group 1 (clustering discussed more in depth later). Samples near the waste rock piles (GW1_18, GW3_18, MW1_18, MW1_20) showing the highest values, varying between 1777–2285 µS/cm (Table S-1, Fig. 10). The groundwater observation well GW4_20 sample had an EC value of 767 µS/cm, differing noticeably from the GW5_18 and GW5_20 values of 72 and 67 µS/cm, respectively. Observation well GW5 is outside the mine environment site. The Levijoki river (RW3, RW6, RW11) has EC values of 58–102 µS/cm, with the lower values from the easternmost measurements and the highest near the mine site.

Field-measured EC values of waters in the sampling locations were compared to the EC values interpreted from the GEM-2 EC data (Fig. 6). In Saattopora, there was a statistically moderate correlation ($p < 0.05$, Pearson $r = 0.418$), likely mainly due to the GEM-2 measurement lines not matching well with the water sampling points. Better correlation was found in the area between and to the north of the waste rock piles. There was no statistically significant correlation between the EC field and GEM-2 EC values in the Kevitsa data.

Dissolved oxygen for the groundwater samples (GW1-GW5) ranged between 3.9 and 12.9 mg/L. The rest of the water samples had a similar range, between 2.7 and 10.7 mg/L. The field temperature measurements reflect the groundwater surface water divide, with groundwater samples ranging between 0.14 (in GW3_18, likely a result of

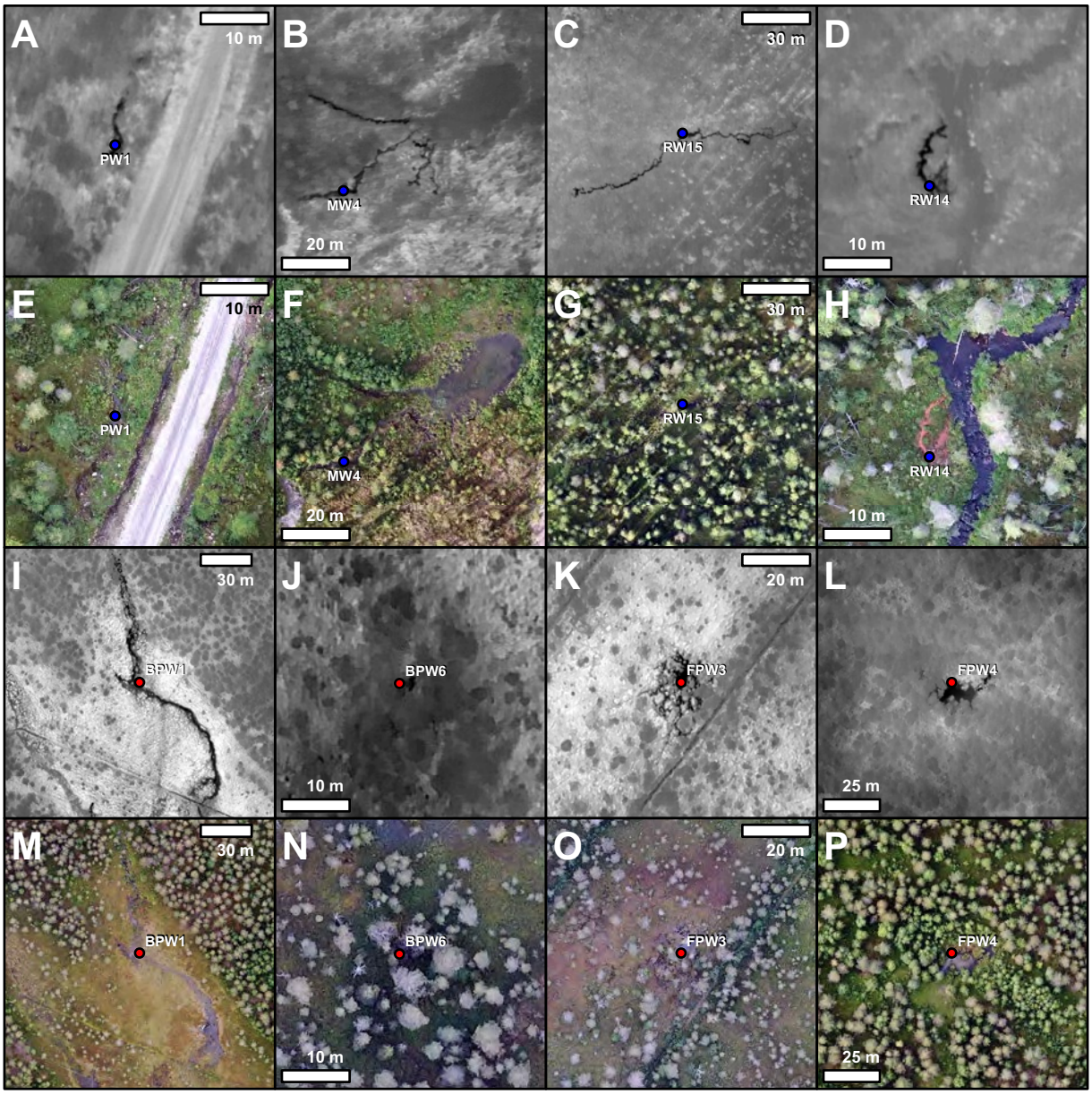

Fig. 5 TIR closeups of some of the identified cold spots from **A**–**D** Saattopora site and **I**-**L** Kevitsa site, with corresponding RGB imagery in **E**–**H** and M-P)

snow/ice in the well) and 3.0 °C measured on 5th and 6th June 2018 and 7.5–8.6 °C in 2020, measured on 9th September (GW4 and GW5). Surface water temperatures ranged between 5.5 and 13.1 °C. Redox values ranged from −27 to 290 mV.

Kevitsa With the Kevitsa sampling locations, the field measurements produced a pH range of 3.7–7.1, an EC range of 24–2199 µS/cm, a DO range of 3.0–11.9 mg/L, and a temperature range of 4.7–15.0 °C. The measurements were carried out on the 31st of August and on the 1st of September 2021. The lowest pH values were found in the bog pond water samples, BPW2 (3.8), BPW3 (3.8), and BPW7 (3.7), as well as the forest pond water sample FPW5 (4.0). The highest EC values were found in the cluster group 1 samples (GW1, MW1, FPW2, and FPW5) with a range of 1835–2616 µS/cm. Cluster group 2 had an EC range of 241–943 µS/cm and cluster group 3 an EC range of 19–250 µS/cm. Redox values ranged from -77.3 to 414.5 mV. The groundwater observation well temperature range of 5.3–9.3 °C (GW1–GW4) was noticeably higher than the 3–4 °C range observed for the groundwaters in northern Finland (Hietula

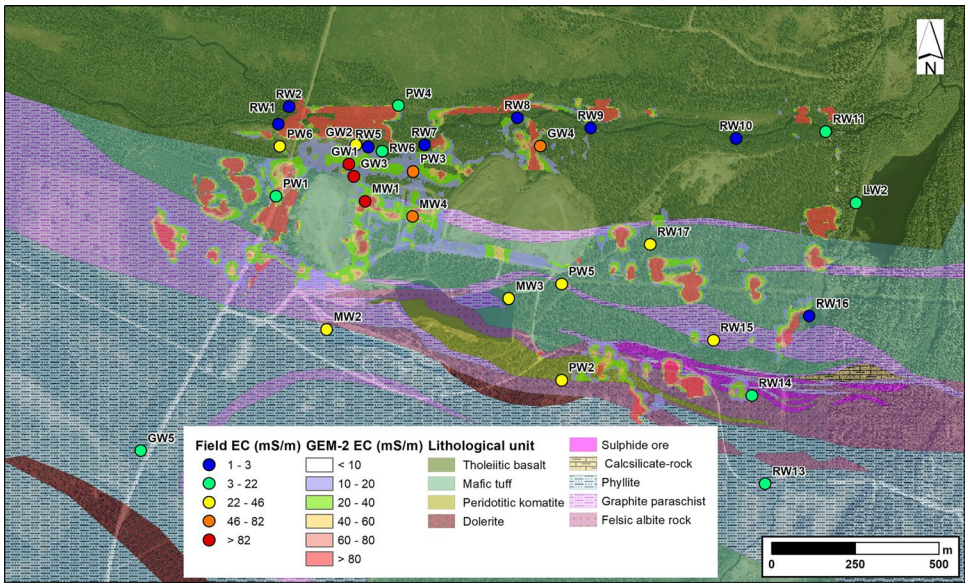

Fig. 6 GEM-2 electrical conductivity (EC) anomalies, EC values at water sampling points and bedrock geology at the Saattopora study site

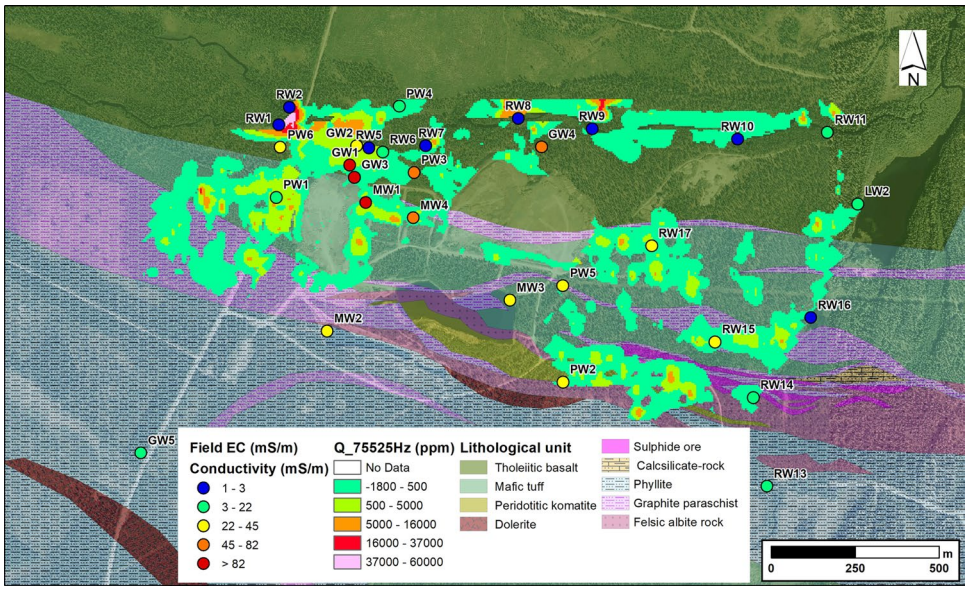

Fig. 7 GEM-2 Quadrature anomalies at the (high) frequency of 75,525 Hz, EC values at water sampling points and bedrock geology at the Saattopora study site

2018). This is likely explained, at least in part, by the sampling method, where a bailer was used to purge the groundwater observation wells. With a more effective groundwater extraction pump for purging, the temperatures would likely have been lower, as the records from the monitoring program show a temperature range of 2.7–5.8 °C for the year 2022 (Boliden 2022).

Main ionic composition of the water samples The ionic balances and the major ion concentrations from the Saattopora and Kevitsa water samples are shown in supplemental Table S-6. The major ion compositions are also presented in Piper diagrams (supplemental Fig. S-2). In Saattopora, the sampled waters were mostly of the Ca-HCO_3 and Ca-Mg-HCO_3 or Mg-SO_4 and Ca-SO_4 type (Fig. S-2 A, B & C). The sulfate-dominated waters were most likely influenced by the waste rock piles where sulfide oxidation occurs (Alakangas et al. 2019).

There were also Ca-Mg-HCO_3 type waters in Kevitsa, but waters with SO_4^{2-} and Cl^- as the main anions dominated. In the Kevitsa area, the natural waters are of the Ca-HCO_3 type; however, a change towards Cl-SO_4 has been discovered near the TSF area, resembling the water composition of the TSF area described by Pienimaa (2019). Waters near the waste rock piles are clearly of the Mg-SO_4 type and differ slightly from Cl-SO_4 dominated process waters of the mine (Pienimaa 2019).

The Saattopora water samples that were classed together in cluster group 4 (Fig. S-2) plot near the Finnish groundwater references with water type Ca-HCO_3. Cluster group 2

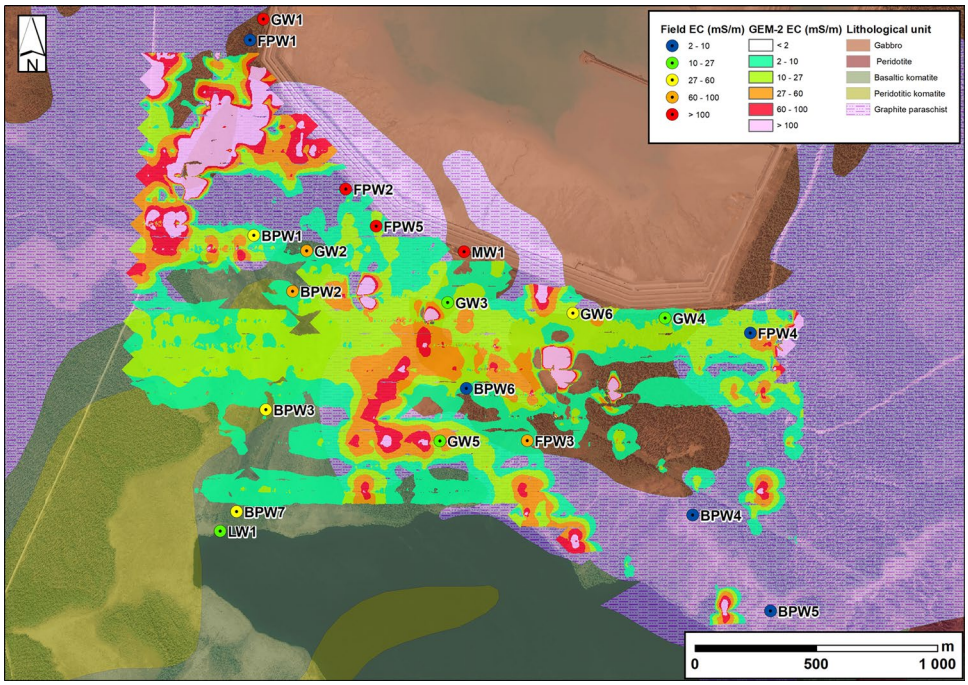

Fig. 8 GEM-2 electrical conductivity (EC) anomalies, EC values at water sampling points and bedrock geology at the Kevitsa study site

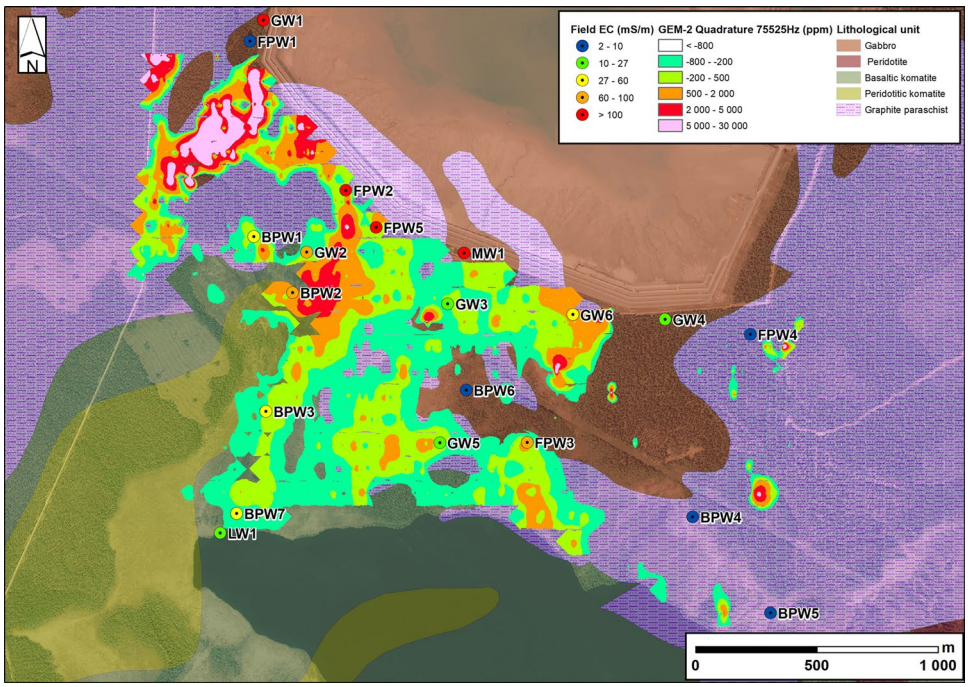

Fig. 9 GEM-2 Quadrature anomalies at the frequency of 75,525 Hz, EC values at water sampling points and bedrock geology at the Kevitsa study site

with water samples GW2_17 and GW2_18 with the Ca-SO_4 water type plot nearer the mine area influenced Mg-SO_4 richer water samples in cluster groups 1 and 3 (MW1, MW2, MW3, MW4, GW4, RW17, PW2, PW3, PW5, PW6) in the Piper graphs A, B, and C (Fig. S-2).

The Kevitsa water samples of cluster group 3 plot near the groundwater references of water type Ca-HCO_3 except for the lake water sample (LW1), which plots nearer to cluster groups 1 and 2. The latter two groups have larger concentrations of Cl and SO_4.

Cluster grouping of water samples Cluster group 1 water samples at both sites correspond with the largest concentrations of the major ions and higher EC values, while the group 4 samples at both sites represent the lowest concentrations and lower EC values (Table 1, Fig. S-2). Concentra-

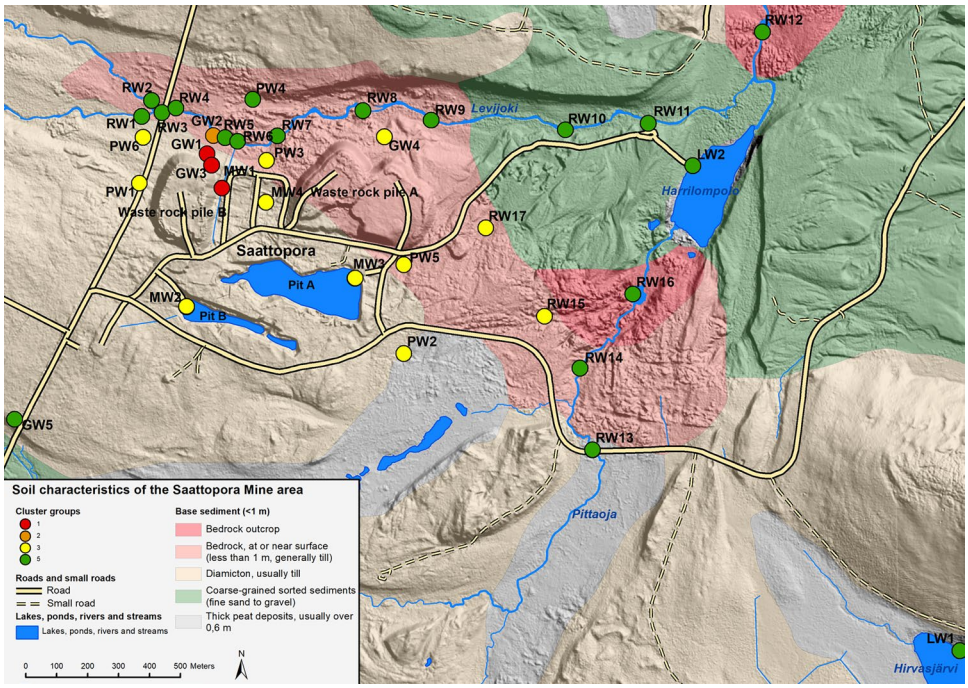

Fig. 10 Soil characteristics of Saattopora mine area with cluster groups. Main ion concentrations, pH, alkalinity, and EC values were used for the cluster analysis. Group 1 presents waters with high concentrations. Concentrations of main ions and EC values change gradually from high (group 1) to low (group 4)

Table 1 Saattopora cluster groups R1-R4 formulated with SPSS (parameters include main ions, EC, pH, and alkalinity). Kevitsa cluster groups R1-R3 formulated with SPSS (parameters include main ions, EC, alkalinity, Co, Ni, and Sr)

Saattopora					Kevitsa		
R1	R2	R3	R4		R1	R2	R3
GW1-17	GW2-18	GW4-17	GW5-18	RW9-16	FPW2	BPW1	BPW4
GW1-18	GW2-17	GW4-20	GW5-20	RW10-16	FPW5	BPW2	BPW5
GW3-17		MW2-16	LW1-16	RW11-20	GW1	BPW3	BPW6
GW3-18		MW2-20	LW2-16	RW12-16	MW1	BPW7	FPW1
MW1-16		MW3-16	PW4-20	RW13-16		FPW3	FPW4
MW1-18		MW3-20	RW1-16	RW13-20		GW2	GW3
MW1-20		PW1-20	RW2-16	RW14-20		GW6	GW4
		PW2-20	RW3-20	RW16-16			GW5
		PW5-20	RW4-16				LW1
		PW6-20	RW5-16				
		RW15-20	RW6-18				
		RW17-20	RW6-20				
		PW3-20	RW7-16				
		MW4-20	RW8-16				

tions and EC values change gradually from group 1 to group 3/4 (Figs. 10, 11).

The hydrogeochemical data for the Saattopora water samples is divided into four different cluster groups with a linkage distance of 2.5 (Figs. S-3 & 11; Table 1). The first group in red includes the sample points near the smaller waste rock pile – MW1, GW1, and GW3. Other groundwater observation wells within or near the mine area are classified 2 (orange) and 3 (yellow); GW2 and GW4 and most of the water samples from or near the mine area are included in cluster group 3. The groundwater reference sample (GW5) is included in group 4 in green, which also includes the river and stream/brook water samples and the lake water sample (RW and LW), as seen in Fig. 10 and Table 1.

The Kevitsa water samples is divided into three groups with a linkage distance of 2.5 (supplemental Fig. S-3 & Fig. 11). The first group in red includes the samples GW1, MW1, FPW2, and FPW5, nearest to the TSF (Fig. 11). The second group in yellow includes pondwater (FPW3, BPW1–3,7) samples from the study site as well as a groundwater observation sample well (GW2) and a spring (GW6). The third group in green includes the lake water sample (LW1), two groundwater observation well samples (GW3

and GW4), and a spring sample (GW5), as well as two pond water samples (FPW1,4 and BPW4,5,6).

Isotopic compositions of analyzed elements The analyzed isotopic compositions of δ^2H, $\delta^{18}O$, $^{87}Sr/^{86}Sr$, and $\delta^{34}S$ from the water samples are presented in Table S-4. The deuterium excess value in per mill is calculated using the δ^2H and $\delta^{18}O$ values with the formula:

$$d - excess = \delta^2H - 8 \times \delta^{18}O \quad (1)$$

The isotopic composition of hydrogen, oxygen, strontium, and sulfur were analyzed from the 2018 and 2020 Saattopora water sampling campaigns. The groundwater reference sample (GW5) was taken from the groundwater observation well southwest of the mine area (Fig. 3). The 2018 reference water sample had a δ^2H value of -104.5 ‰ and $\delta^{18}O$ value of -14.29 ‰, in contrast to 2020 values of -107.8 ‰ and -14.77 ‰, respectively. The 2018 samples were collected in early June after the snowmelt period and the 2020 samples in early September. There is a noticeable variation in the analyzed isotopic compositions of the sampled waters. The δ^2H values ranging from -122.9 to -97.4 ‰ and $\delta^{18}O$ values from -15.36 to -12.56 ‰ (Table S-4). The surface water samples excluding the river Levijoki samples (MW2, MW3, PW5, RW17) had a d-excess ranging from 3.1 to 6.4 ‰. The Kevitsa water samples had δ^2H values ranging from -112.5 to -83 ‰ and $\delta^{18}O$ values from -15.33 to -10.35 ‰, with d-excess values between -0.2 and 10.7.

The local evaporation line (LEL) for Saattopora has endmember MW3_20 representing the most evaporated water (δ^2H -97.4, $\delta^{18}O$ -12.56) and a groundwater endmember near sample GW5_20 (δ^2H -107.8, $\delta^{18}O$ -14.77). Samples that plot on or near the LEL show varying degrees of evaporation (Fig. 12). With the Kevitsa samples, the LEL has the lake water (LW1) as the most evaporated endmember (δ^2H -83, $\delta^{18}O$ -10.35). Samples GW4 and GW5 represent the groundwater endmember on the meteoric water line. Samples that plot on or near the LEL include BPW3, FPW1, BPW7, FPW2, FPW5, MW1, BPW2, GW1, and GW2 (Fig. 12). These evaporated waters likely have their origin from the TSF, since all of the cluster group 1 water samples are found on the evaporation line.

The isotopic composition of $^{87}Sr/^{86}Sr$ in the Saattopora water samples ranged from 0.71257 to 0.75058 and the Sr concentrations ranged from 10.1 to 260.0 µg/L. The $\delta^{34}S$ values ranged from -3.0 to 10.1 ‰, while the sulfur concentration ranged from 1.3 to 474.0 mg/L. The 2018 sampling results of the Saattopora water samples GW 1, GW2, GW3, GW5, MW1, and RW6 are also displayed here (Table S-4).

The $^{87}Sr/^{86}Sr$ values for the sampled Kevitsa water ranged from 0.72522 to 0.76939 and the Sr concentrations ranged from 3.1 to 884.0 µg/L. The highest concentrations are seen in samples GW1, MW1, FPW2, and FPW5. Values for $\delta^{34}S$ in the water samples ranged from 4.4 to 19.8 ‰, while the concentrations of S ranged from 0.3 to 241.0 mg/L. As with Sr, the highest sulfur concentrations are seen in the GW1, MW1, FPW2, and FPW5 samples, which all belong to cluster group 1 (Fig. 11).

At the Saattopora site, samples taken based on the TIR cold spots included MW1, MW4, PW1, PW3, PW6, RW14, RW15, and RW17. Cold spot samples in the Kevitsa site were BPW1–7 and FPW2–5, in addition to the two spring water samples GW5 and GW6 (Fig. 3, Table S-4).

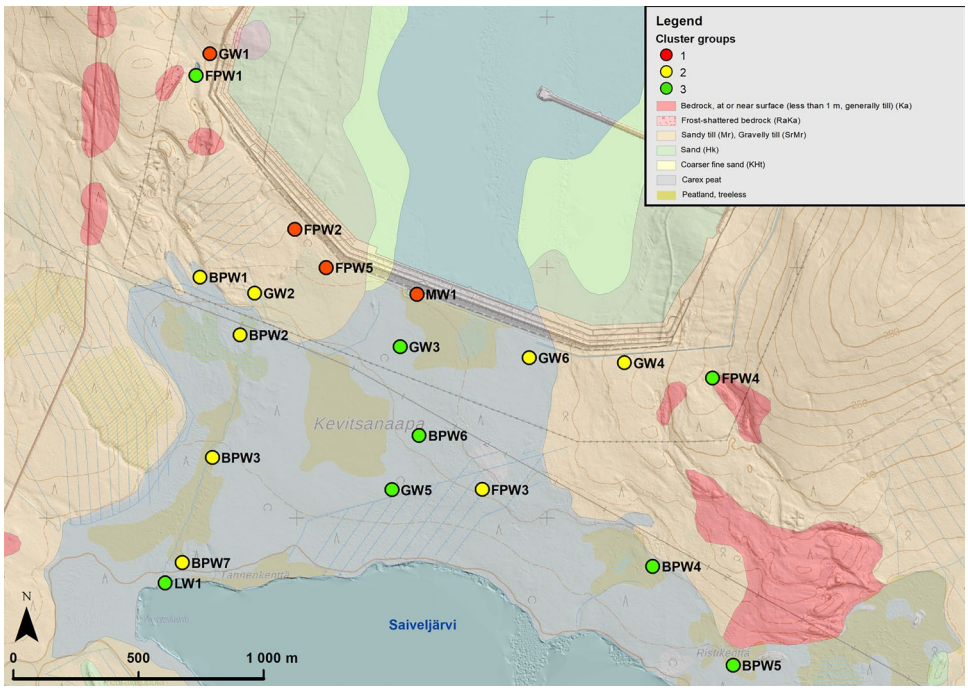

Fig. 11 Soil characteristics of Kevitsa mine area with cluster groups. Main ions, Co, Ni and Sr concentrations, alkalinity, and EC values were used for the cluster analysis. Group 1 presents waters with higher ion concentrations. Concentrations change gradually from higher (group 1) to lower (group3)

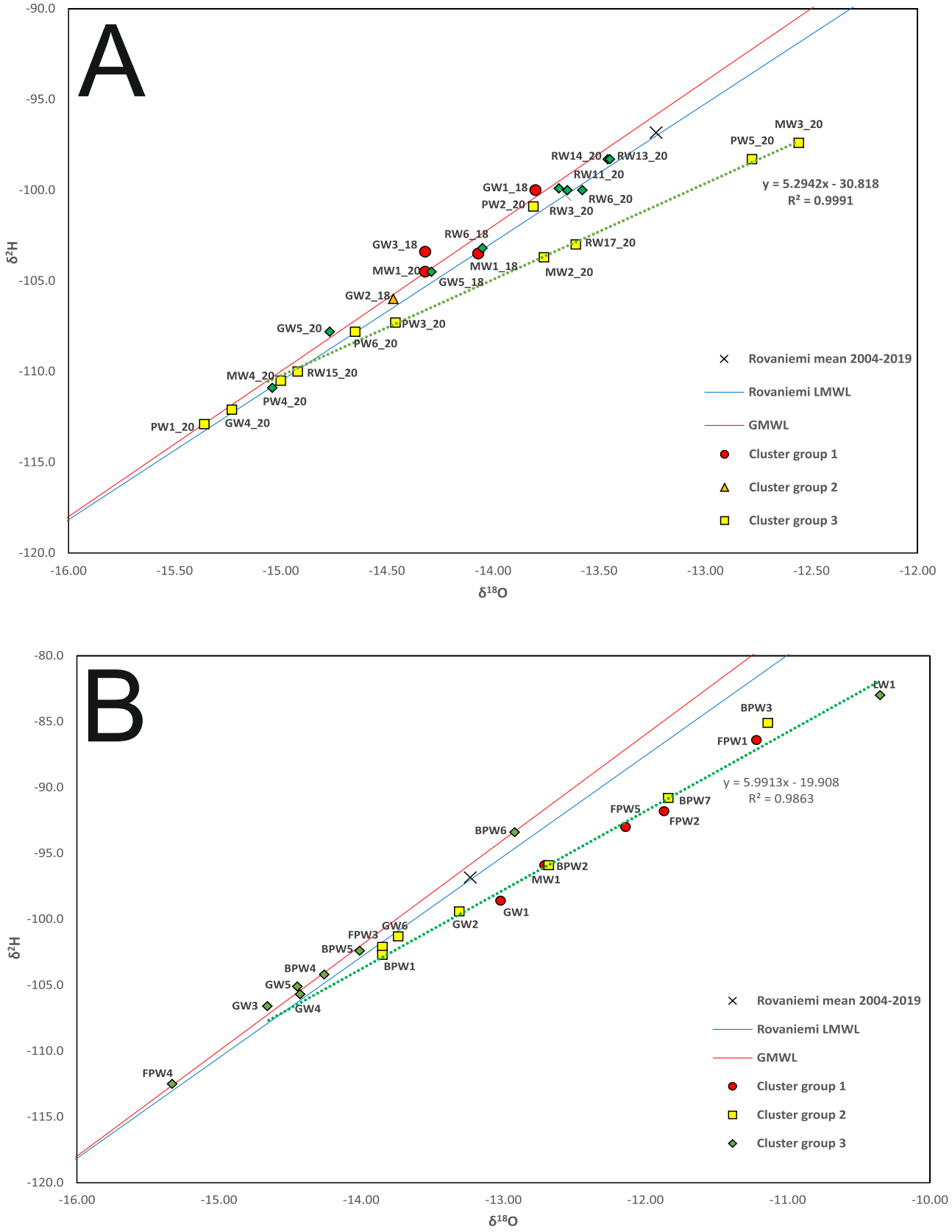

Fig. 12 Isotopic compositions of oxygen and hydrogen against the GMWL and the Rovaniemi LMWL of the 2018 & 2020 water samples in Saattopora **A** and the 2021water samples in Kevitsa **B**

Discussion

Groundwater Discharge Based on TIR Images and Isotopic Compositions of Hydrogen and Oxygen

The TIR images were used to identify locations where the groundwater, which is colder than the surface water, was upwelling or discharging. To evaluate these sites and to distinguish between groundwater and surface water, the isotopic compositions of hydrogen and oxygen from the water samples was then analyzed. The evaporation that occurs from a surface water body causes the δ^2H and $\delta^{18}O$ values to plot below the meteoric water line, which represents the unevaporated waters of meteoric origin. Here the local meteoric water line (LMWL) was produced from the GNIP (Global Network of Isotopes in Precipitation) precipitation samples from Rovaniemi, just less than 200 km south of the study areas (IAEA/WMO GNIP database).

In Saattopora, the water samples found on the LMWL plot below the Rovaniemi precipitation weighted mean. This is also true for the Kevitsa groundwater samples (Fig. 12). The more negative isotopic compositions of hydrogen and oxygen of the water samples reflect the more northerly location of the two study sites compared to Rovaniemi. The variations seen in the δ^2H and $\delta^{18}O$ values of the water samples that plot on the LMWL speaks of the strong seasonality affecting the isotopic compositions of hydrogen and oxygen (Fig. 12), which in turn may be explained by the smaller groundwater bodies at the study sites, especially at Saattopora. The attenuation of seasonality has less effect in smaller groundwater bodies (Kortelainen and Karhu 2004).

The LEL and the LMWL in Saattopora intersect near GW5, PW4, and RW15. GW5 was planned as the reference groundwater sample due to its location outside the mining zone. Sampling spot PW4 was a groundwater puddle and RW15 was from a ditch that has some groundwater discharge. In Kevitsa, the intersection was found near GW3 and GW4, which are groundwater observation wells in the study area. The intersections of the LEL and LMWL represent the mean groundwater composition in these sites (Fig. 12).

The samples that were collected based on cold spots in Saattopora had hydrogen and oxygen isotopic compositions on or very near the LMWL, showing them to be unevaporated water of meteoric origin (Fig. 12). The d-excess values for these samples ranged from 8.10 to 10.14 (Table S-6). The only exception was sample RW17 with a d-excess of 5.88, which was from a ditch with a slow flow of water east of waste rock pile A (Fig. 10, Table S-4). The ditch at this sampling site may have occasional groundwater influence, causing it to show as a cold spot on the day of the TIR imaging.

The Kevitsa cold spot samples (BPW2, BPW3, BPW7, FPW2, and FPW5) had a clear surface water component in them with d-excess values ranging from 3.16 to 5.54, indicating evaporation. As with the exception in Saattopora, these sampling sites may experience varying groundwater influence and showed up as cold spots in the TIR images that were acquired two weeks before the sampling. Additionally, the UAS-TIR images only revealed information on the surface layer of the water (Hare et al. 2015; Isokangas et al. 2017), allowing for challenges in interpreting the data.

This study looked at the benefits of using UAS-TIR images to determine locations of groundwater upwelling and possible surface water – groundwater interaction sites as part of combining various methods in assessing mine site hydrogeology. The use and applicability of TIR images in groundwater and environmental studies has been well documented in recent years (Briggs et al. 2018; Casas-Mulet et al. 2020; Isokangas et al. 2019; Rautio et al. 2018; Young and Pradhanang 2021). TIR surveys are best performed at maximum daily temperatures when the temperature difference between the air and the target surface is greatest, making the thermal signature of groundwater most visible (Loheide and Gorelick 2006). Overcast conditions are deemed best, as they minimize shade-induced temperature anomalies (Rautio et al. 2018). Here, samples were not only taken based on TIR images but also from selected groundwater observation wells and based on the GEM-2 anomalies as well as the general hydrogeological features in the area, i.e. brooks, rivers, or lakes. The TIR images revealed cold spots that were diagnosed as temperature anomalies by brightness value variations.

Hydrogeochemical and isotopic composition analyses of selected elements in sampled waters is a proven method to track various processes in water pathways at mine sites (Larkins et al. 2018). The need for manageability of monitoring can be an important issue at large mine sites, especially in areas with challenging access due to topography and/or terrain.

One of the aims of this study was to produce more feasible ways of producing a sampling plan for monitoring waters at a mine site. The UASs were used to produce TIR images to reveal likely groundwater seepage sites, i.e. cold spots. The potential groundwater influence in a water sample from such a cold spot can be determined by analyzing the isotopic compositions of hydrogen and oxygen. Other than the above-described exceptions, the TIR analyses proved well suited for spotting groundwater-influenced sampling sites. To avoid such outliers as found here, it would be advisable to perform sampling as soon as possible after acquiring the TIR images.

Anomalies Caused by Local Geochemistry in GEM-2 Measurements and the Corresponding Hydrogeochemistry

The conductive black schist mineralization zones and mafic tuff areas controlled the GEM-2 EC results at the study sites and made the interpretation challenging. In Kevitsa, the high frequency quadrature component of GEM-2 results correlated well with the cluster groups, alluding to suitability in tracking the effluent waters (Fig. 10). The weak correlation between the EC values from the water samples and the GEM-2 EC values, mentioned earlier, may be the result of the GEM-2 EC values representing deeper structures (up to 10 m depth) of the soil matter and the influence of the bedrock surface. Thus, the GEM-2 EC values reflect the local bedrock influence, causing variation between the soil conductivity values and EC values of the water samples.

The use of GEM-2 measurements has been moderate in hydrogeological studies in Finland. Elsewhere, the method has been applied to study hydrostratigraphical characterization and hydrogeological features of aquifers (Shah et al. 2008) or contaminant dispersion (Yaccup and Brabham 2012). At mine sites, the conductivity values of effluent waters seem to produce a diagnostic signal that can be used to reveal their flow paths.

Isotopic analyses of Sr and S in support of other methods used here was done to see if they would provide more information on the hydrogeochemical processes, potential mixing of waters, or the local geochemistry in the study areas. Thus, the processes that influence the fractionation of the sulfur isotopes, or the local geochemistry influenced strontium isotopic compositions might then reveal information about the anomalies tracked by the UAS-TIR and GEM-2 methods. At both study sites here, the large variation in the strontium isotopic compositions from the water samples was also connected to the mineralogy of the soil and the bedrock, i.e. the local geochemistry. Similar to the conclusions made from the GEM-2 EC results, the elevated conductivity values were probably caused by the deeper reaches of the soil in the areas of conductive mineral matter (Fig. 6). With sulfur, such connections with the superficial anomalies could be connected to the fractionation of sulfur isotopes by biogeochemical processes. The diverse microbial communities of peatlands, the accumulation of reactive organic matter, and a series of redox processes influence the sulfur species (Porowski et al. 2019). Oxidation of sedimentary sulfides produces negative $\delta^{34}S$ values while sulfides from igneous rocks can have values from −10‰ to + 10‰. Atmospheric sulfur has values from + 4‰ to + 6‰, and dissolution of gypsum or anhydrite can produce values from + 10‰ to + 30‰ (Ingri et al. 1997; Liu et al. 2017).

The process of microbial sulfate reduction under anaerobic conditions is the most important process influencing the fractionation of the isotopic composition of sulfur. It removes the lighter isotope ^{32}S from the solution and produces H_2S gas (Isokangas et al. 2019; Larkins et al. 2018). This explains the smell of sulfur in some of the sampling locations in Kevitsa (mentioned in the sampling field notes). Additional explanation for the enrichment of $\delta^{34}S$ both in Kevitsa and Saattopora is that the isotopic analysis method used turns all the S-components into sulfate and sulfide (Paris 2013), which would produce more negative $\delta^{34}S$ values, was not analyzed separately. The variation in the isotopic composition of sulfur can be seen for example in the GW5 sample in Saattopora, where the 2018 sampling has a value of 10.1 and the 2020 sampling 3.8 (Table S-4). The field measurements show a 2018 redox value of 85.6 mV compared to the 2020 value of 204 mV (Table S-2). PCA analysis was performed with the main ions, selected trace elements, field measurements, and isotopic compositions of sulfur ($\delta^{34}S$). The Saattopora redox values correlated with $\delta^{34}S$ values whereas the Kevitsa $\delta^{34}S$ values correlated with the main ion and sulfur concentrations as well as the field EC values (supplemental Tables S-7 and S-8).

The strontium isotopic compositions in the Ni-PGE ore in Kevitsa ranges from 0.709 to 0.711 (Luolavirta et al. 2018). Such references could not be found for the Saattopora ore, but according to Kaislaniemi (2011), the regional geology in central Lapland has a more radiogenic strontium isotopic composition, with values ranging from 0.7236 to 0.7424. The variation in the isotopic composition of Sr in the water samples was large at both Saattopora (0.71257–0.75058) and Kevitsa (0.72522–0.76939) (Table S-4). The notable variation speaks of the geological complexity of the studied mine areas, and the local geochemistry is reflected in the $^{87}Sr/^{86}Sr$ compositions of the water samples. Mafic minerals tend to lower the values for $^{87}Sr/^{86}Sr$, while felsic minerals will cause increased $^{87}Sr/^{86}Sr$ values (Clark & Fritz 1997; Kietäväinen et al. 2013; Shand et al. 2009). This was seen in these two study sites with paraschist rock types as well as felsic albite rock in Saattopora (Fig. 6).

The dissolved concentrations of Sr and S from the water samples are presented against their respective isotopic compositions in Fig. 13. This is commonly done, e.g. to assess mixing of waters or to trace the effects of geochemical processes on isotopic compositions. The isotopic compositions of strontium of the water samples of the two study sites have no clear endmembers to determine mixing of waters. This is reflected in Saattopora where groundwater sample GW5 taken from the well outside the mine site produced two different compositions from the 2018 and 2020 sampling (Fig. 13). This observation well was found to have a rodent trapped inside it during the 2018 sampling. It was removed and the well was purged on the previous day prior to sampling. Still, this might explain the variation in the results

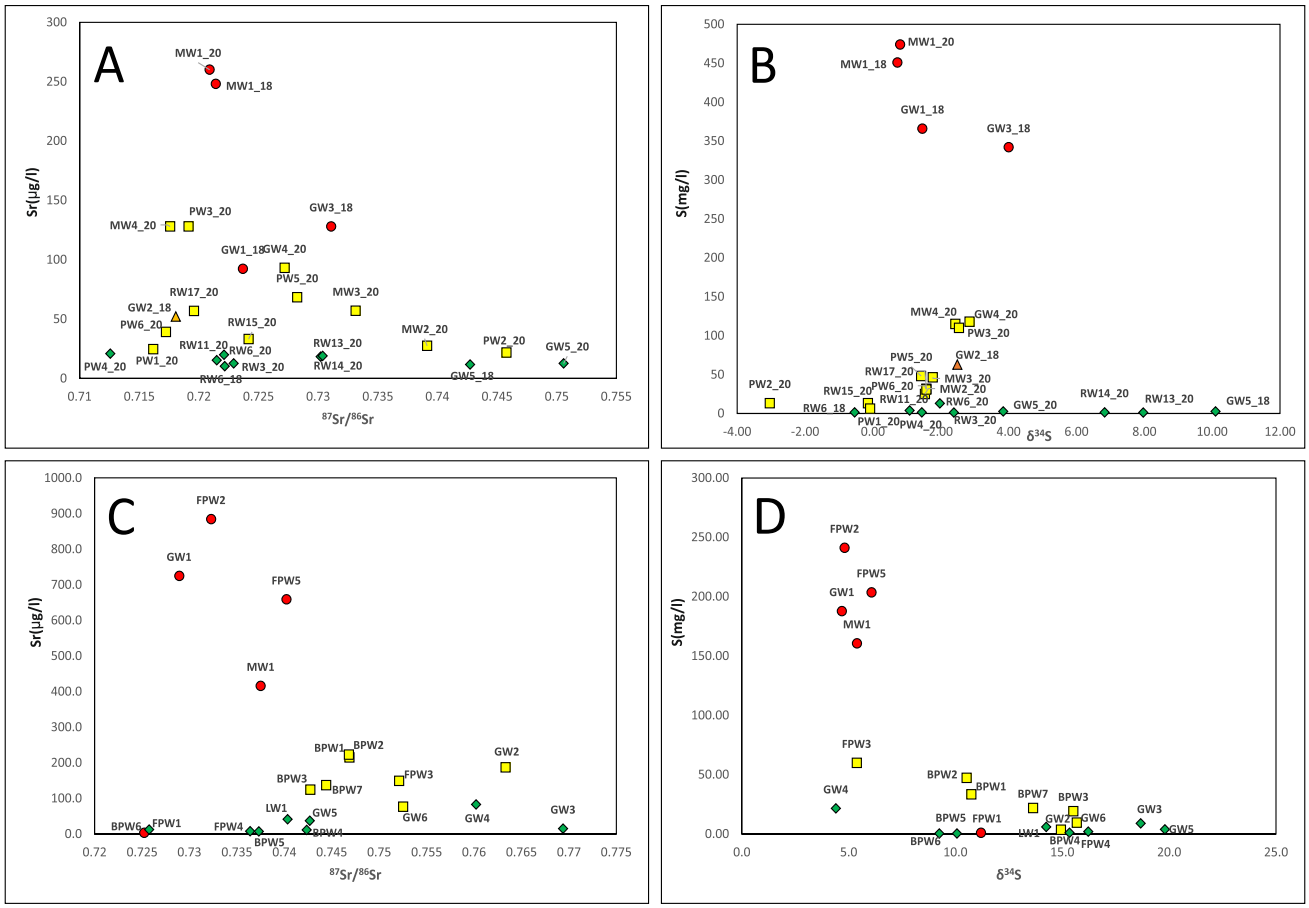

Fig. 13 Isotopic compositions of Sr and S against their concentrations in the water samples in Saattopora (A -Strontium, B – Sulfur) and Kevitsa (C – Strontium, D – Sulfur). Color codes correspond to the different cluster groups (Figs. 12, 13 & S2; Table 1) and the labels reveal the various water types (GW-groundwater, MW-mine water, RW-river water, PW-pond water, FPW-forest pond water, BPW-bog pond water, LW-lake water)

since it speaks to the well not being fully protected from such incidents.

The Applicability of the Methods Used to Focus Water Sampling

With the hydrogeochemistry results, clustering of water samples produced maps where the concentrations and conductivity of the main ions, two parameters that are closely linked to each other, mostly dictated the division of the cluster grouping (Figs. 12, 13). The highest concentrations and conductivity values were from Saattopora in the samples taken near the waste rock piles (Fig. 10). The elevated values (cluster groups 1 and 2) at Kevitsa occur near the TSF and along the small brook leading into lake Saiveljärvi (Fig. 11). The elevated GEM-2 conductivity values also concentrate near the waste rock piles in Saattopora (Fig. 6), although there are anomalies caused by the local geochemistry further east of the waste rock piles. The elevated GEM-2 quadrature values at Kevitsa tell a similar story to the cluster grouping (Fig. 9).

At the Kevitsa study site, the combination of UAS-TIR data and GEM-2 high frequency soil conductivity values of the top sediment reveal anomalies potentially caused by the TSF. Focusing the sampling to these anomalies reveals a good correlation to the cluster grouping with higher concentrations of major ions and EC in the sampled waters (Fig. 11). The isotopic compositions of oxygen and hydrogen can be seen as backing this assumption, since the cluster group 1 samples occur on the LEL (Fig. 12). This indicates that the water originates from the TSF where evaporation has fractionated the isotopic composition. The isotopic composition of sulfur is probably influenced mostly by the sulfide ore body with a median $\delta^{34}S$ of + 4 ‰ (Luolavirta et al. 2018) and potentially oxidation of sulfide/pyrite, causing lighter values. This is also seen in the Saattopora values of sulfur isotopic compositions, with even lighter values (Table S-4). In contrast to the Kevitsa site, the Saattopora mine site did not have a TSF, and the sulfide ore has been analyzed as

having $\delta^{34}S$ values ranging from 2.23 to 4.08 ‰ (Mänttäri 1995). The waste rock piles at Saattopora are the source of the higher metal concentrations seen in the solute concentrations of Sr and S in samples GW1, GW2, GW3, and MW1 (Fig. 10; Table S-4). The combination of pre-sampling methods reveals anomalies that differ from that at Kevitsa and it seems the strongest flow of effluent waters is towards the river Levijoki, as seen in the GEM-2 soil conductivity anomalies (Figs. 6, 7). This discharge, however, is masked in the samples taken from the river due to its flow rate. The use of UAS-TIR at the Saattopora study site reveals areas of potential groundwater discharge, but tracking the effluent water pathways from the waste rock piles does not paint as clear a picture as at the Kevitsa site.

The use of TIR images in determining locations of groundwater upwelling has a very good track record (Anderson 2005; Casas-Mulet et al. 2020; Isokangas et al. 2019; Rautio et al. 2018; Young and Pradhanang 2021). Differentiating groundwater and surface water samples with the isotopic compositions of oxygen and hydrogen is a tried and tested method. The cold spots found in the TIR images in this study proved to be either unevaporated water of meteoric origin or from water reservoirs that had a clear groundwater influence.

The added benefit of performing the GEM-2 measurements remains debatable based on the apparent conductivity (EC) values at these study sites. The anomalies caused by the local mineral matter and the potential of the GEM-2 device in reaching EC values below the topsoil can produce challenges in interpreting the results as shown here with only modest correlation between the EC values from GEM-2 data and from the EC values analyzed from the water sampling sites. However, the high frequency GEM-2 quadrature values, which mostly represent the topsoil, seems to have a better potential for revealing effluent water discharge.

In addition to the anomalies induced by local geochemistry and interpreted using the GEM-2 data, the mineralogy of the soil and bedrock also played an important role in causing variations in the strontium isotopic compositions observed in the water samples. The sulfur isotopic compositions revealed biogeochemical processes and redox conditions along the water flow paths but were also determined by the source material, which can be unique at mine sites and cause noticeable variations in the results (Kim et al. 2019).

Conclusions and Implications

Cost-efficient water sampling plans for a mine site can be achieved when combining various methods to estimate the flow paths of natural and effluent waters at a study site. In this study, uncrewed aerial systems (UAS) produced thermal infrared images (TIR) that were analyzed along with GEM-2 conductivity data from two mine sites in the high-latitude subarctic zone in Finland: the Saattopora abandoned Cu-Au site and the active Cu-Ni-PGE mine site of Kevitsa. Anomalies from the pre-sampling data were merged with the available hydrogeological knowledge of the study sites, and a sampling plan was created to assess possible flow paths of mine effluent waters. The water samples were analyzed for their hydrochemical components as well as isotopic compositions of oxygen, hydrogen, strontium, and sulfur.

The TIR images proved useful in detecting groundwater upwelling at both study sites. Isotopic analyses of hydrogen and oxygen revealed the influence of groundwater in water samples taken at the sites of the TIR anomalies, i.e. cold spots. Isotopic compositions of Sr and S in the sampled waters provided information on local geochemistry and biogeochemical processes, including redox conditions, at the two study sites. Notably, there was marked differences in the isotopic compositions of both Sr and S in the water samples from the two sites. This can be partly explained by the complex local geochemistry of the mine sites, where rock types such as paraschist and felsic albite influenced the Sr isotopic composition. Additionally, biogeochemical processes, such as the oxidation and reduction of sulfur in the groundwater, contributed to the observed variations.

The GEM-2 results revealed local geochemical anomalies, especially in the conductive black schist mineralization zones, which interfered with the initially intended tracking of electrical conductivity (EC) anomalies related to effluent waters at the mine sites. The topsoil-aimed high frequency quadrature component correlated with the cluster grouping of hydrochemical parameters from the sampled waters, especially at the Kevitsa study site. The combined use of TIR images, GEM-2, and hydrogeochemistry can be a powerful tool in hydrogeological studies, particularly in challenging terrain. However, site-specific geological anomalies may pose challenges in the interpretation of data.

Supplementary Information The online version contains supplementary material available at https://doi.org/10.1007/s10230-024-01020-1.

Acknowledgements This study was part of the "Drone-based monitoring of mine environments" 2020-2022 project funded by the European Regional Development Fund, and co-funded by AFRY Finland Oy, Geobotnia Oy, Mitta Oy, Boliden Kevitsa Mining Oy, AA Sakatti Mining Oy, Radai Oy, Maa- ja vesitekniikan tuki ry., Oulun rakentamistekniikan säätiö, Inno-Cad Oy ja Fortum Waste Solutions Oy. The other supporting financiers were K.H. Renlund's Foundation, and Strategic Research Council of the Academy of Finland. The 2016-2018 data was collected during the "Development, Evaluation and Optimization of Measures to Reduce the Impact on the Environment from Mining Activities in Northern Regions (Min-North, 2016–2018)"-project, funded by the Interreg Nord 2014-2020 program. Special thanks to the laboratory personnel at GTK and particularly to Yann Lahaye for contributing to the analytical methodology of isotopic compositions of

strontium and sulfur and to Nina Hendriksson for her consultations on the isotope geochemistry.

Funding Open Access funding provided by Geological Survey of Finland.

Data Availability The data supporting the findings are available upon reasonable request from the corresponding author.

References

Alakangas L, Salifu M, Rasmussen TM, Heino N, Hyvönen E, Karlsson T, Panttila H, Pietilä R, Tornivaara A, Turunen K, Lu J, Fu S, Bui MT, Heiderscheidt E, Postila H, Leiviskä T, Ronkanen A-K, Kujala K, Khan U, Gogoi H (2019) Min-North: development, evaluation and optimization of measures to reduce the environmental impact of mining activities in northern regions. Retrieved from the Luleå University of Technology website: https://urn.kb.se/resolve?urn=urn:nbn:se:ltu:diva-75722

Almeida HD, Gomes Marques MC, Sant'Ovaia H, Moura R, Espinha Marques J (2023) Environmental impact assessment of the subsurface in a former W-Sn mine: integration of geophysical methodologies. Minerals 13(1):55. https://doi.org/10.3390/MIN13010055

Anderson MP (2005) Heat as a groundwater tracer. Groundwater 43:951–968. https://doi.org/10.1111/j.1745-6584.2005.00052.x

Autio A, Ala-Aho P, Rossi PM, Ronkanen AK, Aurela M, Lohila A, Korpelainen P, Kumpula T, Klöve B, Marttila H (2023) Groundwater exfiltration pattern determination in the sub-arctic catchment using thermal imaging, stable water isotopes and fully integrated groundwater-surface water modelling. J Hydrol 626:130342. https://doi.org/10.1016/j.jhydrol.2023.130342

Banerjee BP, Raval S, Cullen PJ (2015) Unmanned aerial vehicles for mine environment monitoring. In: Proc, 3rd International Future Mining Conf, The Australasian Institute of Mining and Metallurgy, Melbourne, pp 137–144

Boaga J, Viezzoli A, Cassiani G, Deidda GP, Tosi L, Silvestri S (2020) Resolving the thickness of peat deposits with contact-less electromagnetic methods: a case study in the Venice coastland. Sci Total Environ 737:139361. https://doi.org/10.1016/j.scitotenv.2020.139361

Boliden (2022) Annual report. Retrieved from https://www.boliden.com/fi/operations/mines/boliden-kevitsa/vuosiraportit [in Finnish]

Briggs MA, Dawson CB, Holmquist-Johnson CL, Williams KH, Lane JW (2018) Efficient hydrogeological characterization of remote stream corridors using drones. Hydrol Process. https://doi.org/10.1002/hyp.13332

Canfield DE (2001) Biogeochemistry of sulfur isotopes. Rev Mineral Geochem 43:607–636. https://doi.org/10.2138/gsrmg.43.1.607

Casas-Mulet R, Pander J, Ryu D, Stewardson MJ, Geist J (2020) Unmanned aerial vehicle (UAV)-based thermal infra-red (TIR) and optical imagery reveals multi-spatial scale controls of cold-water areas over a groundwater-dominated riverscape. Front Environ Sci 8:64. https://doi.org/10.3389/fenvs.2020.00064

Choe E, van der Meer F, van Ruitenbeek F, van der Werff H, de Smeth B, Kim KW (2008) Mapping of heavy metal pollution in stream sediments using combined geochemistry, field spectroscopy, and hyperspectral remote sensing: a case study of the Rodalquilar mining area. SE Spain Remote Sens Environ 112(7):3222–3233. https://doi.org/10.1016/j.rse.2008.03.017

Conant B (2001) Relationship between groundwater flux, geochemical conditions, and biodegradation of a PCE plume discharging through a riverbed. In: American Geophysical Union Fall Meeting

Dansgaard W (1964) Stable isotopes in precipitation. Tellus 16:436. https://doi.org/10.3402/tellusa.v16I4.8993

Dugdale SJ, Kelleher CA, Malcolm IA, Caldwell S, Hannah DM (2019) Assessing the potential of drone-based thermal infrared imagery for quantifying river temperature heterogeneity. Hydrol Process 33:1152–1163. https://doi.org/10.1002/HYP.13395

Faure G, Mensing TM (2005) Principles and applications. John Wiley & Sons, Hoboken

FMI, Ilmatieteenlaitos (2022) https://www.ilmatieteenlaitos.fi/ilmastollinen-vertailukausi-1981-2010. Accessed 9 March 2023

Glaser B, Antonelli M, Chini M, Pfister L, Klaus J (2018) Technical note: mapping surface-saturation dynamics with thermal infrared imagery. Hydrol Earth Syst Sci 22:5987–6003. https://doi.org/10.5194/HESS-22-5987-2018

Grisso R, Alley M, Groover G (2009) Precision farming tools: GPS navigation. Virginia Cooperative Extension Precision Farming Series, 7

Hare DK, Briggs MA, Rosenberry DO, Boutt DF, Lane JW (2015) A comparison of thermal infrared to fiber-optic distributed temperature sensing for evaluation of groundwater discharge to surface water. J Hydrol 530:153–166. https://doi.org/10.1016/j.jhydrol.2015.09.059

Hayashi M, Rosenberry DO (2002) Effects of ground water exchange on the hydrology and ecology of surface water. Ground Water 40:309–316. https://doi.org/10.1111/j.1745-6584.2002.tb02659.x

Hietula S (2018) Suomen matalapohjaveden lämpötila, siihen vaikuttavat tekijät ja valtakunnallisen lämpötilakartoituksen käyttökelpoisuus geoenergiapotentiaalin arvioinnissa. MS thesis, Univ of Helsinki. https://helda.helsinki.fi/items/853abea1-9079-4e9e-ac7b-92758516b4f9 [in Finnish]

Hinton MJ, Schiff SL, English MC (1994) Examining the contributions of glacial till water to storm runoff using two- and three-component hydrograph separations. Water Resour Res 30:983–993. https://doi.org/10.1029/93WR03246

Huang H, Won IJ (2003) Real-time resistivity sounding using a hand-held broadband electromagnetic sensor. Geophys 68(4):1224–1231

IAEA/WMO GNIP database. https://www.iaea.org/services/networks/gnip. Accessed 10 October 2023

Ingri J, Torssander P, Andersson PS, Mörth CM, Kusakabe M (1997) Hydrogeochemistry of sulfur isotopes in the Kalix river catchment, northern Sweden. Appl Geochem 12:483–496. https://doi.org/10.1016/S0883-2927(97)00026-7

Isokangas E, Rossi PM, Ronkanen A-K, Marttila H, Rozanski K, Kløve B (2017) Quantifying spatial groundwater dependence in peatlands through a distributed isotope mass balance approach. Water Resour Res 53:2524–2541. https://doi.org/10.1002/2016WR019661

Isokangas E, Davids C, Kujala K, Rauhala A, Ronkanen AK, Rossi PM (2019) Combining unmanned aerial vehicle-based remote sensing and stable water isotope analysis to monitor treatment peatlands of mining areas. Ecol Eng 133:137–147. https://doi.org/10.1016/j.ecoleng.2019.04.024

Kaislaniemi L (2011) Estimating the distribution of strontium isotope ratios (87Sr/86Sr) in the Precambrian of Finland. Bull Geol Soc Finland 83:95–113

Karan SK, Samadder SR, Maiti SK (2016) Assessment of the capability of remote sensing and GIS techniques for monitoring reclamation success in coal mine degraded lands. J Environ Manage 182:272–283. https://doi.org/10.1016/j.jenvman.2016.07.070

Kendall C, Coplen TB (2001) Distribution of oxygen-18 and deuterium in river waters across the United States. Hydrol Process 15:1363–1393. https://doi.org/10.1002/hyp.217

Kenoyer GJ, Anderson MP (1989) Groundwater's dynamic role in regulating acidity and chemistry in a precipitation-dominated lake. J Hydrol 109:287–306. https://doi.org/10.1016/0022-1694(89)90020-6

Kietäväinen R, Ahonen L, Kukkonen IT, Hendriksson N, Nyyssönen M, Itävaara M (2013) Characterisation and isotopic evolution of saline waters of the Outokumpu Deep Drill Hole, Finland – implications for water origin and deep terrestrial biosphere. Appl Geochem 32:37–51. https://doi.org/10.1016/j.apgeochem.2012.10.013

Kim DM, Yun ST, Yoon S, Mayer B (2019) Signature of oxygen and sulfur isotopes of sulfate in ground and surface water reflecting enhanced sulfide oxidation in mine areas. Appl Geochem 100:143–151. https://doi.org/10.1016/j.apgeochem.2018.11.018

Korkalo T (2006) Gold and copper deposits in central Lapland, northern Finland, with special reference to their exploration and exploitation. OuluREPO. https://oulurepo.oulu.fi/handle/10024/35050. Accessed 17 January 2024

Korkka-Niemi K, Kivimäki AL, Lahti K, Nygård M, Rautio A, Salonen VP, Pellikka P (2012) Observations on groundwater-surface water interactions at river Vantaa, Finland. Manag Environ Qual 23:222–231. https://doi.org/10.1108/14777831211204958/full/xml

Kortelainen N, Karhu J (2004) Regional and seasonal trends in the oxygen and hydrogen isotope ratios of Finnish groundwaters: a key for mean annual precipitation. J Hydrol 285:143–157. https://doi.org/10.1016/j.jhydrol.2003.08.014

Korvuo E (1997) The Saattopora gold ore and the Pahtavuoma Cu-Zn-U occurrences in the Kittilä region, northern Finland. Geol Survey Finland Guide 43:21–25

Krabbenhoft DP, Bowser CJ, Anderson MP, Valley JW (1990) Estimating groundwater exchange with lakes: 1. the stable isotope mass balance method. Water Resour Res 26:2445–2453. https://doi.org/10.1029/WR026I010P02445

Lahermo P, Tarvainen T, Hatakka T, Backman B, Juntunen R, Kortelainen N, Lakomaa T, Nikkarinen M, Vesterbacka P, Väisänen U, Suomela P (2002) Tuhat kaivoa - Suomen kaivovesien fysikaaliskemiallinen laatu vuonna 1999 (summary: One thousand wells-the physical-chemical quality of Finnish well waters in 1999). Report of Investigation 155, Geological Survey of Finland, Espoo [in Finnish]

Larkins C, Turunen K, Mänttäri I, Lahaye Y, Hendriksson N, Forsman P, Backnäs S (2018) Characterization of selected conservative and non-conservative isotopes in mine effluent and impacted surface waters: Implications for tracer applications at the mine-site scale. Appl Geochem 91:1–13. https://doi.org/10.1016/j.apgeochem.2018.01.005

Lehtonen M, Airo M-L, Eilu P, Hanski E, Kortelainen V, Lanne E, Manninen T, Rastas P, Räsänen J, Virransalo P (1998) Lapin vulkaniittiprojektin raportti (summary in English: The stratigraphy, petrology and geochemistry of the Kittilä greenstone area, northern Finland). Geological Survey of Finland, Report of Investigation 140 [in Finnish]

Lerssi J, Niemi S, Suppala I (2016) GEM-2 – new generation electromagnetic sensor for near surface mapping. Extended abstract in Near Surface, 22nd European Meeting of Environmental and Engineering Geophysics, Barcelona, Spain

Liu J, Li S, Zhong J, Zhu X, Guo Q, Lang Y, Han X (2017) Sulfate sources constrained by sulfur and oxygen isotopic compositions in the upper reaches of the Xijiang River, China. Acta Geochim 36:611–618. https://doi.org/10.1007/S11631-017-0175-1/figures/4

Loheide SP, Gorelick SM (2006) Quantifying stream–aquifer interactions through the analysis of remotely sensed thermographic profiles and in situ temperature histories. Environ Sci Technol 40(10):3336–3341. https://doi.org/10.1021/es0522074

Luolavirta K, Hanski E, Maier W, Lahaye Y, O'Brien H, Santaguida F (2018) In situ strontium and sulfur isotope investigation of the Ni-Cu-(PGE) sulfide ore-bearing Kevitsa intrusion, northern Finland. Miner Depos 53:1019–1038. https://doi.org/10.1007/s00126-018-0792-6

Manninen T, Hyvönen E, Johansson P, Kontio M, Pänttäjä M, Väisänen U (1996) Kevitsan alueen geologia. Geological Survey of Finland report [in Finnish]

Mänttäri I (1995) Lead isotope characteristics of epigenetic gold mineralization in the Palaeoproterozoic Lapland greenstone belt, northern Finland. Geological Survey of Finland vol 381. http://tupa.gtk.fi/julkaisu/bulletin/bt_381.pdf

McKenna PB, Lechner AM, Phinn S, Erskine PD (2020) Remote sensing of mine site rehabilitation for ecological outcomes: a global systematic review. Remote Sens 12(21):3535. https://doi.org/10.3390/RS12213535

McNeill JD (1980) Electrical conductivity of soils and rocks. Geonics Ltd

Minh DT, Dung NB (2023) Applications of UAVs in mine industry: a scoping review. J Sustain Min 22(2):128–146. https://doi.org/10.46873/2300-3960.1384

Molnar F, Lahaye Y, O'Brien H, Kurhila M, Hulkki H (2019) The Saattopora orogenic Au-Cu deposit, central Lapland greenstone belt, Finland: fluid sources and timing of hydrothermal processes. Conference paper. Life with Ore Deposits on Earth – 15th SGA Biennial Meeting 2019, Volume 2

Paris G, Sessions AL, Subhas AV, Adkins JF (2013) MC-ICP-MS measurement of δ34S and Δ33S in small amounts of dissolved sulfate. Chem Geol 345:50–61. https://doi.org/10.1016/j.chemgeo.2013.02.022

Pellicori DA, Gammons CH, Poulson SR (2005) Geochemistry and stable isotope composition of the Berkeley pit lake and surrounding mine waters, Butte, Montana. Appl Geochem 20:2116–2137. https://doi.org/10.1016/j.apgeochem.2005.07.010

Peltoniemi M (1982) Characteristics and results of an airborne electromagnetic method of geophysical surveying. Geological Survey of Finland Bulletin 321

Pernu T (1991) Model and field studies of direct current resistivity measurements with the combined (half-Schlumberger) array ANM, NMB. Acta Universitatis Ouluensis, Series A, Scientiae Rerum Naturalium 221

Pienimaa T (2019) Rikastushiekka-altaan suotovesien kulkeutuminen Kevitsan kaivosalueella. MS thesis, Univ of Oulu. https://oulurepo.oulu.fi/handle/10024/13112 [in Finnish]

Pietilä R, Eloranta T, Räisänen M-L, Tornivaara A, Törmänen T, Väisänen U (2014) Rikkiyhdisteiden vaikutusten arviointi - Sulkahankkeen loppuraportti. Geological Survey of Finland, research report [in Finnish]

Porowski A, Porowska D, Halas S (2019) Identification of sulfate sources and biogeochemical processes in an aquifer affected by peatland: insights from monitoring the isotopic composition of groundwater sulfate in Kampinos National Park, Poland. Water 11(7):1338. https://doi.org/10.3390/W11071388

Pöyry (2011) Kevitsan kaivoksen laajennus. Ympäristövaikutusten arviointiselostus. https://www.ymparisto.fi/fi/osallistu-ja-vaikuta/ymparistovaikutusten-arviointi/kevitsan-kaivoksen-laajennus-sodankyla. Accessed 12 September 2023 [in Finnish]

Qu S, Wang C, Yang N, Duan L, Yu R, Zhang K, Li M, Sun P (2023) Large-scale surface water-groundwater origins and connectivity in the Ordos Basin, China: insight from hydrogen and oxygen isotopes. Environ Res. https://doi.org/10.1016/J.ENVRES.2023.116837

Rastas P, Huhma H, Hanski E, Lehtonen MI, Paakkola J, Mänttäri I, Härkönen I (2001) U-Pb isotopic studies on the Kittilä greenstone area, central Lapland, Finland. In: Vaasjoki M (ed) Radiometric age determinations from Finnish Lapland and their bearing on the timing of Precambrian volcano-sedimentary sequences. Geological Survey of Finland Special Paper 33

Rauhala A, Tuomela A, Davids C, Rossi PM (2017) UAV remote sensing surveillance of a mine tailings impoundment in sub-arctic conditions. Remote Sens 9(12):1318. https://doi.org/10.3390/rs9121318

Rautio A, Korkka-Niemi K (2015) Chemical and isotopic tracers indicating groundwater/surface-water interaction within a boreal lake catchment in Finland. Hydrogeol J 23:687–705. https://doi.org/10.1007/s10040-015-1234-5

Rautio A, Kivimäki AL, Korkka-Niemi K, Nygård M, Salonen VP, Lahti K, Vahtera H (2015) Vulnerability of groundwater resources to interaction with river water in a boreal catchment. Hydrol Earth Syst Sci 19:3015–3032. https://doi.org/10.5194/HESS-19-3015-2015

Rautio A, Korkka-Niemi K, Salonen VP (2018) Thermal infrared remote sensing in assessing groundwater and surface-water resources related to Hannukainen mining development site, northern Finland. Hydrogeol J. https://doi.org/10.1007/s10040-017-1630-0

Santaguida F, Luolavirta K, Lappalainen M, Ylinen J, Voipio T, Jones S (2015) The Kevitsa Ni-Cu-PGE deposit in the lapland greenstone belt in Finland. In: Maier W, Lahtinen R, O'Brien H (eds) Mineral Deposits of Finland. Elsevier Science B.V, Amsterdam, pp 195–210

Sares M, Hauff P, Peters DC, Coulter DW (2004) Characterizing sources of acid rock drainage and resulting water quality impacts using hyperspectral remote sensing – examples from the upper Arkansas River basin, Colorado. Advanced Integration of Geospatial Technologies in Mining and Reclamation, December

Shah SD, Smith BD, Clark AK, Payne JD (2008) An integrated hydrogeologic and geophysical investigation to characterize the hydrostratigraphy of the Edwards aquifer in an area of northeastern Bexar County, Texas. USGS Scientific Investigations Report

Shand P, Darbyshire DPF, Love AJ, Edmunds WM (2009) Sr isotopes in natural waters: applications to source characterisation and water–rock interaction in contrasting landscapes. Appl Geochem 24:574–586. https://doi.org/10.1016/J.APGEOCHEM.2008.12.011

Solantie R, Joukola M (2001) Evapotranspiration 1961–1990 in Finland as function of meteorological and land-type factors. Boreal Environ Res 261–273

Swayze GA, Smith KS, Clark RN, Sutley SJ, Pearson RM, Vance JS, Hageman PL, Briggs PH, Meier AL, Singleton MJ, Roth S (2000) Using imaging spectroscopy to map acidic mine waste. Environ Sci Technol 34(1):47–54. https://doi.org/10.1021/es990046w

Tomaštík J, Mokroš M, Surový P, Grznárová A, Merganič J (2019) UAV RTK/PPK method - an optimal solution for mapping inaccessible forested areas? Remote Sens. https://doi.org/10.3390/RS11060721

Turunen K, Räsänen T, Hämäläinen E, Hämäläinen M, Pajula P, Nieminen SP (2020) Analysing contaminant mixing and dilution in river waters influenced by mine water discharges. Water Air Soil Pollut 231:1–15. https://doi.org/10.1007/S11270-020-04683-Y/FIGURES/8

Valjus T, Huotari T, Lerssi J, Markovaara-Koivisto M, Tarvainen T (2017) Geophysical study of a potential source of secondary raw materials - the Aijala mine tailings area, southern Finland. 23rd European Meeting of Environmental and Engineering Geophysics Sep 2017 Volume 2017:1–5

Winkelmann I, Thomas M, Vogl K (2001) Aerial measurements on uranium ore mining, milling and processing areas in Germany. J Environ Radioact 53(3):301–311. https://doi.org/10.1016/S0265-931X(00)00138-7

Witten A, Won IJ, Norton S (1997) Imaging underground structures using broadband electromagnetic induction. J Environ Eng Geophys 2(2):105–114

Won IJ, Keiswetter DA, Fields GRA, Sutton LC (1996) GEM-2: a new multifrequency electromagnetic sensor. J Environ Eng Geophys 1:129–137. https://doi.org/10.4133/JEEG1.2.129

Yaccup R, Brabham P (2012) Ground electromagnetic survey (GEM-2) technique to map the hydrocarbon contaminant dispersion in the subsurface at Barry Docks, Wales, UK. Conference paper - AWAM International Conference on Civil Engineering and Geohazard Information Zonation

Young KS, Pradhanang SM (2021) Small unmanned aircraft (sUAS)-deployed thermal infrared (TIR) imaging for environmental surveys with implications in submarine groundwater discharge (SGD): methods, challenges, and novel opportunities. Remote Sens 13(7):1331. https://doi.org/10.3390/rs13071331

Yu T-L, Wang B-S, Shen C-C, Wang P-L, Yang TF, Burr GS, Chen Y-G (2017) Improved analytical techniques of sulfur isotopic composition in nanomole quantities by MC-ICP-MS. Anal Chim Acta 988:34–40. https://doi.org/10.1016/j.aca.2017.08.012